*Review*

# The Joining of Copper to Stainless Steel by Solid-State Welding Processes: A Review

Gaurang R. Joshi [1,2,3], Vishvesh J. Badheka [4], Raghavendra S. Darji [3,4,5], Ankit D. Oza [6], Vivek J. Pathak [7], Dumitru Doru Burduhos-Nergis [8,*], Diana Petronela Burduhos-Nergis [8,*], Gautam Narwade [9] and Gopinath Thirunavukarasu [9]

1    Department of Mechanical Engineering, Marwadi University, Rajkot 360003, Gujarat, India
2    Fusion Blanket Division, Institute for Plasma Research, Ahmedabad 382428, Gujarat, India
3    Laxmipati Engineering Works Limited, Surat 394221, Gujarat, India
4    Department of Mechanical Engineering, School of Technology, Pandit Deendayal Energy University, Gandhinagar 382007, Gujarat, India
5    Department of Metallurgy and Materials Engineering, The M S University, Baroda 390001, Gujarat, India
6    Department of Computer Sciences and Engineering, Institute of Advanced Research, The University for Innovation, Gandhinagar 382426, Gujarat, India
7    Department of Automobile Engineering, Marwadi University, Rajkot 360003, Gujarat, India
8    Faculty of Materials Science and Engineering, Gheorghe Asachi Technical University of Iasi, 700050 Iasi, Romania
9    School of Mechanical Engineering, Dr. Vishwanath Karad MIT World Peace University, Kothrud, Pune 411038, Maharashtra, India
*    Correspondence: doru.burduhos@tuiasi.ro (D.D.B.-N.); diana.burduhos@tuiasi.ro (D.P.B.-N.)

**Abstract:** Joining immiscible materials such as copper and stainless steel together is a significant concern due to distinct mechanical and metallurgical properties across the joint line, such as melting points, the coefficient of linear thermal expansion, and thermal conductivity. The joint properties of copper to stainless steel welds are in great demand for various mechanical components of the international thermonuclear experimental reactor, ultra-high vacuum system, plan wave linear-accelerator or linac structure, and heat exchanger. These dissimilar-metals joints offer excellent flexibility in design and production, leading to a robust structure for many cutting-edge applications. Hence, the present article reviews the copper to stainless steel joining mechanism under different solid-state processing conditions. The present understanding says that defect-free strong joints between the dissimilar metals are systematically possible. Apart from this understanding, the authors have identified and highlighted the gaps in the research exploration to date. Moreover, a sustainable methodology to achieve a desirable weld of copper to stainless steel depends on favorable processing conditions.

**Keywords:** copper; dissimilar; welding; explosive; review; stainless steel; diffusion; intermixing; solubility; processing

## 1. Introduction—Joining of Copper to Stainless Steel Bimetallic System

Robust and compact structures are the key characteristics demanded for all modern engineering products [1–4]. The realization of both robustness and compactness in a component is possible only if it is made from multiple materials [5–11]. Joints of dissimilar materials give different combinations of mechanical and metallurgical characteristics in a product. Thus, bimetallic joints [12–17] are necessary, especially in a vacuum [18–23] and cryogenic systems [24–27]. Because of the unique combination of distinct properties, copper/stainless-steel bimetals are in great demand [28–34]. Stainless steel (SS) combines high strength, low thermal diffusivity, reasonable ductility, and eliminates ductile-to-brittle transitional behaviour. Whereas copper (Cu) embedded high thermal conductivity, better corrosion resistance, and intrinsic absence of ductile-to-brittle transitional behaviour. In this

connection, Cu to SS bimetallic amalgamation is the need of the hour for the applications detailed above. Hence, understanding the joining mechanism of Cu to SS under different processing techniques is essential and unavoidable.

However, metallurgical incompatibility (solubility, multiple elements, liquid metal characteristics, and solidification pattern) between copper and stainless steel is significant. The diverse nature of both materials is dominant during fusion welding processes. However, considerable effort has been made to join copper to stainless steel via fusion welding processes [35–47]. Overall, it is safe to conclude that the metallurgy of copper to stainless steel joints must be the researcher's focus when welding them with fusion welding processes. Stainless steel is an alloy of Fe-Cr-Ni (along with C, Si, Mn, S, P, and Cu), whereas copper is a metal element. Both have the same face-centred cubic crystal structure. However, that of copper is inherent, while that of stainless steel is a product of the addition of nickel to Fe, which eliminates the ductile-to-brittle transitional behaviour of Fe. Similarly, copper's corrosion resistance is in-built, while stainless steel it is resistant due to the presence of chromium. Moreover, nickel and chromium improve the mechanical properties. The ternary phase diagram of Fe, chromium and nickel [48] indicated the same (see Figure 1), i.e., that these are responsible for forming stainless steel. The temperatures at which iron (1539 °C), chromium (1907 °C), and nickel (1484 °C) melt are higher than copper (1084 °C). The thermo-physical properties such as viscosity, surface tension, thermal conductivity, and heat accumulation capacity of ferrous-chromium-nickel alloys (stainless steel) are necessary to consider in heat and mass transport processes, i.e., fusion welding. The properties mentioned above (precisely viscosity) lead to complexity in its estimations, measurements, and calculations. Nonetheless, viscosity has been studied (see Figure 2) earlier [49]. The iron's viscosity improves with the addition of chromium, while pure nickel holds lower viscosity than that of Fe-Cr alloy (overall viscosity of the stainless steel is improved/high). Fe-Cr alloy indicated the highest viscosity (see Figure 2). Similarly, the pure copper's viscosity during the fusion welding process (since copper's phase changed from solid to liquid during the welding and again from liquid to solid during solidification, post welding) is very low (see Figure 3) [50]. It signifies the heterogeneous metal flow of copper and stainless steel in a liquid state
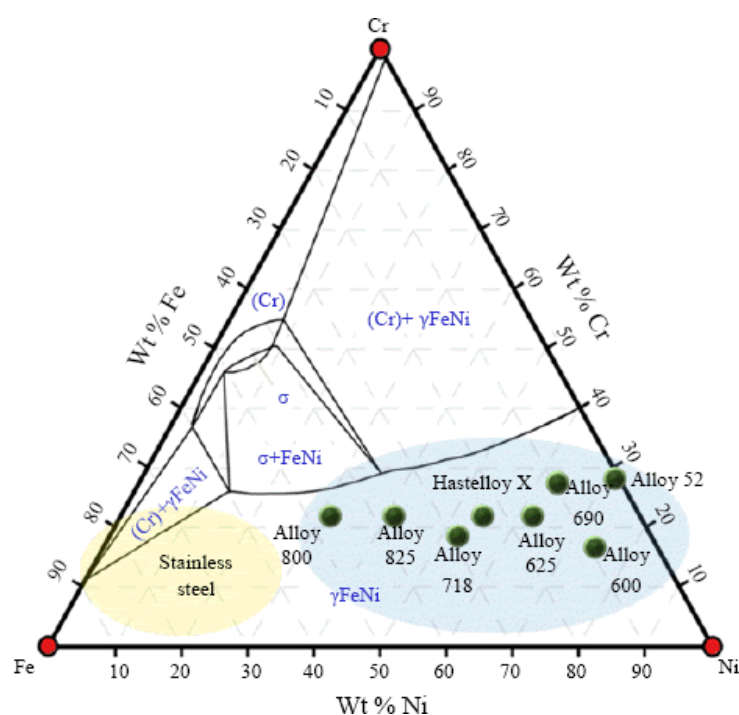


**Figure 1.** Fe-Ni-Cr ternary phase diagram. Reprinted from Ref. [48]. Copyright © 2022 by The Korean Welding and Joining Society.
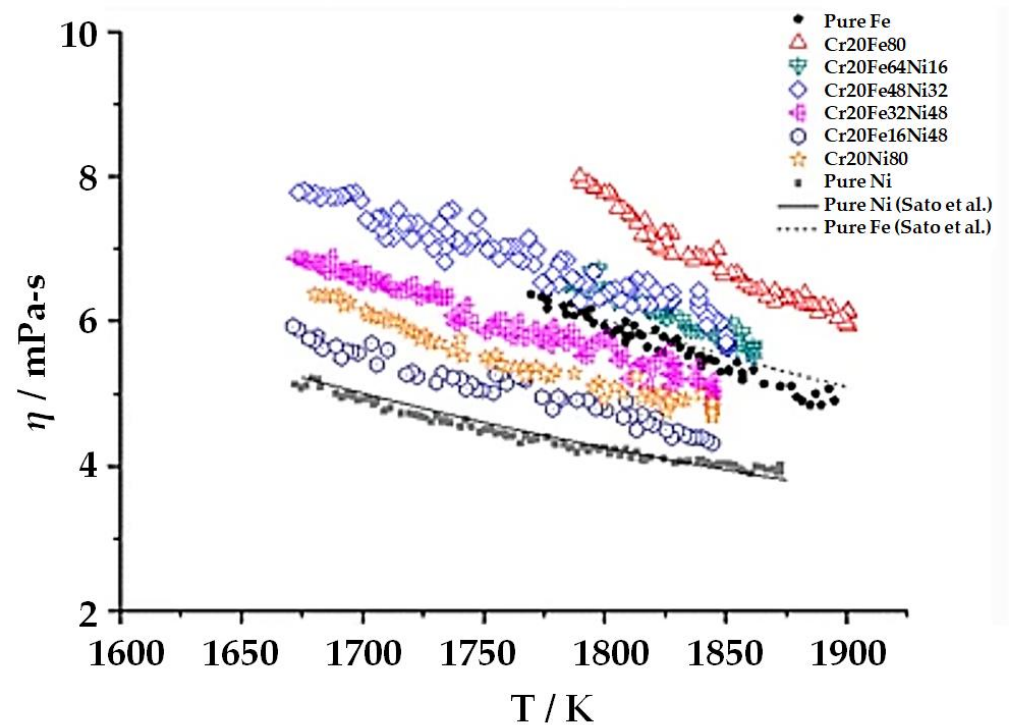
**Figure 2.** Measured viscosities of various Cr-Fe-Ni alloys as a function of temperature, including pure Fe and Ni [49].
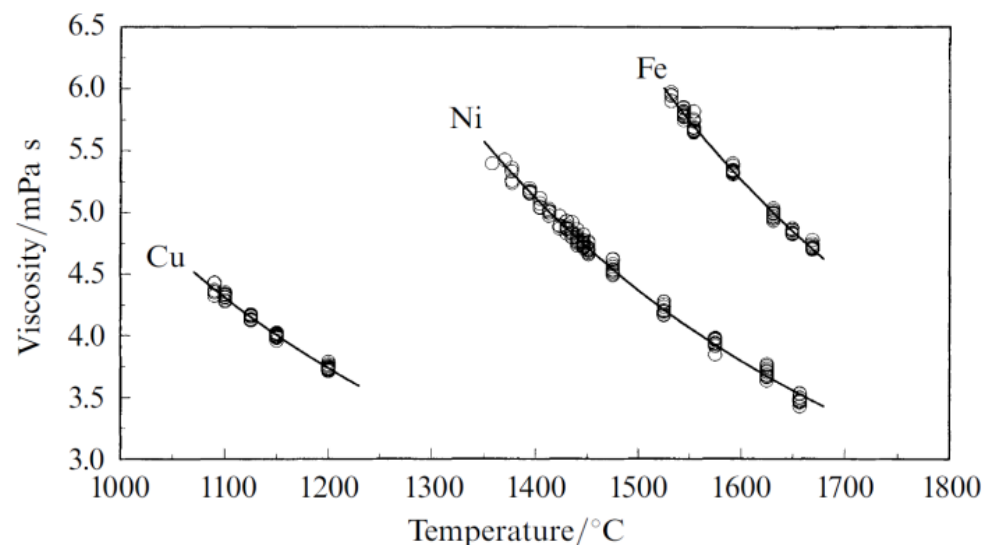


**Figure 3.** Measured Viscosities of Cu, Ni and Fe by Oscillating Viscometer [50].

Based on the material's behaviour in a liquid state while fusion welding, proper fluid flow is essential to efficiently weld either metals or alloys. Copper and nickel are the examples that have been welded successfully [51–55] despite vast differences in viscosities (see Figure 3). Mutual solubility plays a vital role in obtaining better macro and microstructural bonding, i.e., even after favourable flow conditions of the materials during fusion welding. However, the complete miscibility of copper and nickel does not guarantee a good joint. The high fluidity of copper and high viscosity of nickel are equally prone to defects. The turbulence created by extremely fluid copper in its liquid state may be exposed to environmental contamination, leading to porosities and cracks. On the contrary, because of the presence of Ni, the excess fluidity might be reduced by the Ni since it has higher

viscosity that of Cu. This can produce defect-free joints in case liquid Ni dominates the fluid flow.

Similarly, dense nickel results in a lack of sidewall fusion due to its excess viscous weld pool and movement of the weld pool towards the sidewalls is difficult because of the sluggish weld pool. This means that the weld pool's stability is necessary to obtain proper formation of the weld pool. This, in turn, is a sign of a sound (defect-free) weld joint.

However, the fluid flow of copper and stainless-steel are highly unpredictable due to (1) differences in the flow characteristics of copper, nickel, chromium, and iron; and (2) complete mutual immiscibility (see Figure 4) [50]. Hence, defective welded regions of the Cu/SS joints are unavoidable due to the inherent high turbulence of the immiscible liquid metal flow. This is the reason for solidification cracking or porosity. The above make welding method very difficult, requiring close control over the combination of processes, properties and parameters. However, the efficient joining of copper to stainless steel is still possible by using welding torch oscillation [56–60]. This is a less-explored research area which aims to join the above materials by fusion welding processes. However, it is complicated to weld the above-mentioned materials together using a fusion welding process, i.e., due to the aforementioned fusion-associated challenges.
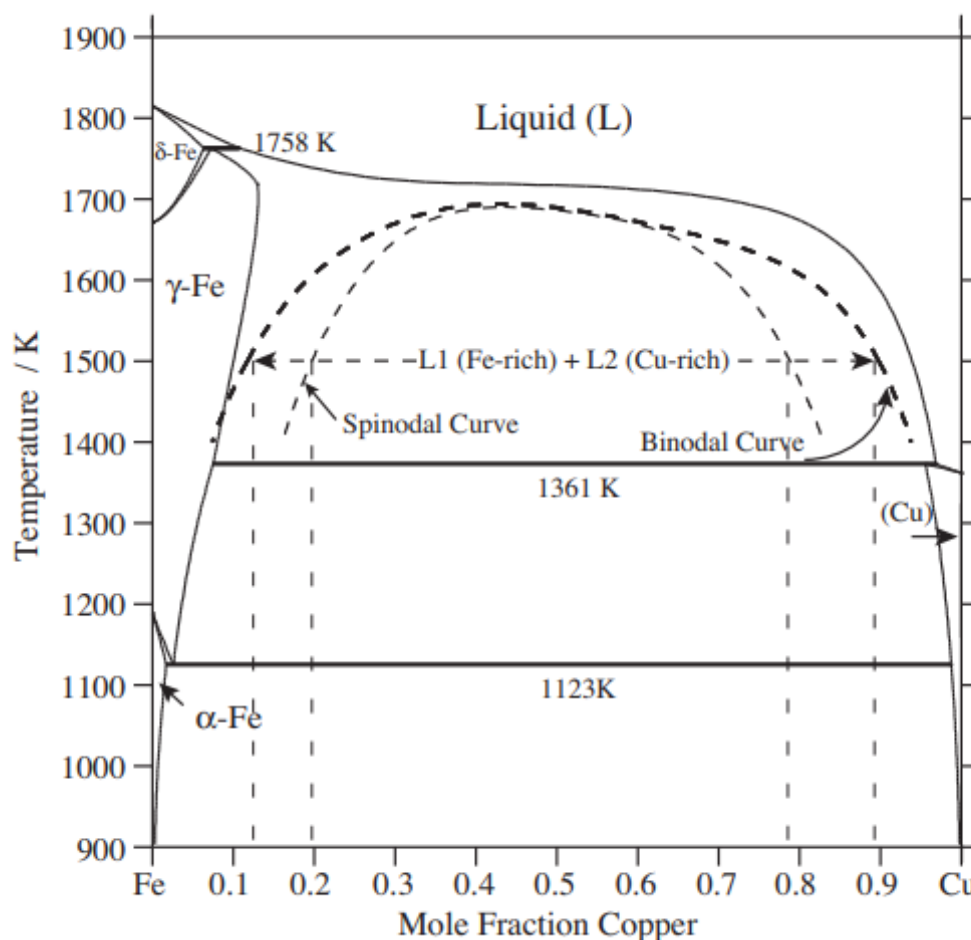


**Figure 4.** Binary Fe–Cu phase diagram with metastable liquid miscibility gap. Reprinted from Ref. [55]. Copyright © 2022 by Elsevier.

Fusion welding of Cu to SS has issues as mentioned above; it is important to report that there is not only a single issue but a series of problems to encounter. To eliminate these challenges, solid-state welding processes are the best choice since they eliminate the issues of fusion welding. In solid-state welding processes, the weld area experiences the temperature above recrystallization, but below melting point [61–68]. In fact, the

temperature during the process is generally far below the melting point. In turn, the scientific community should seek the minimal adverse effect of fusion on the joint as well as trying to reduce the heterogeneity in viscosity, miscibility, melting point, thermal conductivity, and thermal expansion. Hence, researchers have considered solid-state joining methods [69–125] for the bimetallic joints of Cu/SS. Their works are reviewed in the subsequent sections.

## 2. Solid-State Welding of Copper/Stainless Steel Bimetallic Joint

The fusion of copper and stainless-steel faces several challenges which are not limited to miscibility (mutual solubility) (see Figure 4) and distinct properties across the faying surfaces. The mismatch of thermal induced stresses, complex surface tension, and solidification of multiple elements together demand close control and in-depth analysis while considering joining copper with stainless steel. It is essential to discover an optimal processing window for efficient welding of the dissimilar metals. Solid-state joining techniques avoid the fusion of both copper and stainless steel, which eventually reduces associated challenges due to microstructural differences and differences in physical properties [126–133]. This is why various solid-state joining methods are explored by researchers to join copper/stainless-steel. Here, the joint characteristics are compared and discussed throughout the subsequent sections.

### 2.1. Hot Isostatic Pressing of Copper/Stainless Steel Bimetallic Joint

Hot isostatic pressing (HIP) of copper/stainless-steel bimetallic joints is emphasized to address the need of structural components in the design and realization of an international thermonuclear experimental reactor (ITER), especially for the first wall and divertor [70,91,134–136] (see Figure 5) applications. Table 1 summarizes some of the published work in this topic of interest. High heat flux is the primary concern while designing such components [113]. The hypervapotron [122,137–142] is a device which can mitigate the effect of heat flux up to 20–30 MW/m$^2$ on the entire structure of the fusion reactor. Copper alloy acts as a heat sink [143–148] while austenitic stainless steel plays its role as a structural component [123,149–153]. Hence, sustainable joining technology for the mentioned application is necessary. HIP has been selected as a potential joining technique for Cu/SS bimetallic material amalgamation [124]. Extensive research and development (R & D) works were carried out on the Cu/SS joining by HIP (see Table 1). The effect of processing parameters has been assessed on the scale of resulting mechanical and metallurgical properties [124]. The effect of surface polishing and surface roughness on the joining process is discussed in a research paper [124]. In addition to this, the joining of Cu/SS by HIP can be divided into three sections; (1) using interlayer(s) [74,123,124] (2) without interlayer(s) [72,73,75–77,123,125,154] and (3) using heat treatment process variations [73,78–80,83,91,102,122]. Vital factors considered in the joining are temperature (900–1050 °C), pressure (100–150 MPa) and holding-time (70–240 min) [72,73,75,76,83,122,124]. HIP experiments of Cu/SS bimetallic joint using the above different combinations of levels of the factors resulted in acceptable mechanical and metallurgical properties, such as tensile strength (300–415 MPa), elongation (6–16%) and impact toughness (200–600 J/cm$^2$) [124]. Based on the results obtained, it is worthwhile to conclude that the combination of optimum parameters in the range mentioned above can meet the developmental requirements of Cu/SS bimetallic joints for ITER. Thus, HIP is a reliable manufacturing process in the realization of the first wall and divertor components of ITER.

**Table 1.** Summary of literature on the HIP of Cu/SS bimetallic joint.

| Substrate | Thickness (mm) | Joint Design | Parameters | Testing Method | Maximum Obtained Properties of the Joint | Reference |
|---|---|---|---|---|---|---|
| Joint 1 CuAl15/316 SS Joint 2 CuNiBe/316 SS Joint 3 CuAl25/316 SS | 6/6, 15/10, 15/10 | Not reported | Joint 1 & 3 Temperature; 982 °C Pressure: 102 MPa Holding time: 2 h Joint 2 Temperature; 927 °C Pressure: 102 MPa Holding time: 2 h Aged at 500 °C for six h | Tensile test Shear strength test Microstructure SEM EDX AES TEM | UTS (MPa): 290 for joint 1 Shear strength (MPa): 120–125 for joint 2 | [89] |
| DSCu (GlidCop® AL-15 and AL-25)/SS | 1.5 | Tube-plate joint | Temperature; 980 °C, 1030 °C, 1050 °C Pressure: 150 MPa Holding time: 2 h | Tensile test, SEM Microstructure Charpy impact test Fatigue strength test Fracture toughness test Crack propagation test EPMA analysis Microhardness, Heat flux test | Optimum process temperature: 1050 °C | [153] |
| Joint 1 GlidCop A125/316 LN SS Joint 2 Cu-Cr-Zr/316 LN SS Joint 3 GlidCop A125/316 SS | Joint 1 25/40 | Not reported | Joint 1 Temperature (°C); 920, 1000 Pressure (MPa): 100, 140 Holding time (min) 70, 180 Joint 2 Temperature: 1000 °C Pressure: 140 MPa Holding time: 70 min Joint 3 Temperature (°C); 1050 Pressure (MPa): 150 Holding time (h): 2 | Tensile test Microstructure | UTS: 415 MPa Optimum condition Joint 3 | [80] |
| Joint 1 DSCu/316LN SS Joint 2 DSCu/316L SS Joint 3 CuCrZr/316LN SS | Not reported | Not reported | Joint 1 Temperature (°C); 920–1040 Pressure (MPa): 120–140 Holding time (h): 2–4 Joint 2 Temperature (°C); 1050 Pressure (MPa): 150 Holding time (h): 2 Joint 3 Temperature (°C): 920, 1000 Pressure (MPa): 120, 130 Holding time (h): 3, 1 Interlayer: Fe−42%Ni, Ni | Tensile test Microstructure SEM EPMA Impact toughness Fatigue test Fracture toughness | UTS (MPa): 400 % EL: 16 Fracture toughness (J/m²): 12.2 | [76] |
| DSCu/316 SS | Not reported | Not reported | Temperature (°C); 800–1000 Pressure (MPa): 100, 120 Holding time (h): 2–4 | Tensile test Microstructure Fatigue test EDX | UTS (MPa): 408 JE (%): >100 % EL: 16 Optimum condition Temperature (°C); 980 Pressure (MPa): 100 Holding time (h): 2 | [82] |
| Joint 1 CuNiBe/316L Joint 2 CuAl25/316L | Not reported | Not reported | Fixed parameter Pressure (MPa): 101 Holding time (h): 2 Joint 1 Temperature (K); 1245 Joint 2 Temperature (K); 1255 | SEM EDX Microhardness | The significant change in hardness reported | [83] |
| CuCrZr/316 L SS | 7.2/12 | Over lap | Temperature (°C); 900 Pressure (MPa): 130 Holding time (h): 2 | Tensile test, SEM Charpy impact test Microstructure, EDX | UTS (MPa): 321 Impact toughness (J/cm²): 104 | [74] |
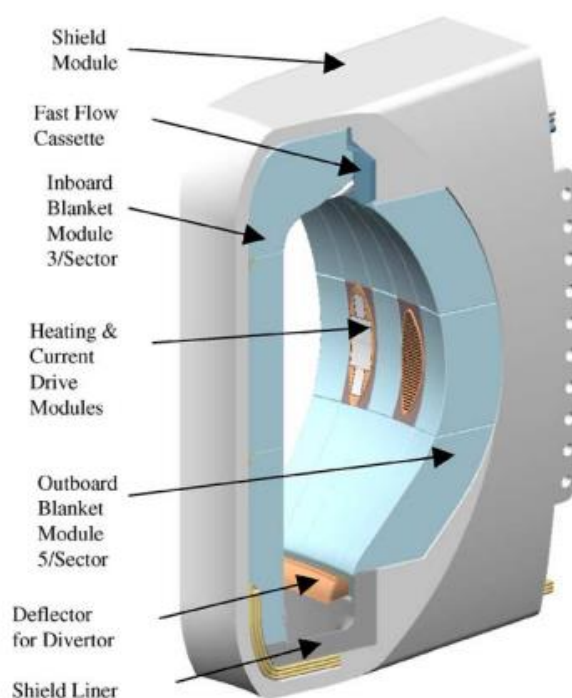
**Figure 5.** Chamber components: first wall and divertor, blanket and shield. Reprinted from Ref. [136]. Copyright © 2022 by Elsevier.

Leedy et al. [83] reported the highest tensile property for the joints of Cu–25%Al and 316 grade SS. In this study, powder-form of Cu–25%Al/316SS showed significant degradation in tensile properties. Cold working of the powder form is not possible, resulting in the restricted interaction of the fine dispersion of oxide particles with high dislocation density. The oxide particles obstruct the dislocation movement, leading to stress concentration, and limits the grain growth. These are the reasons for the reduction in mechanical strength. The oxygen inclusion in the powder Cu/SS joint acts as a diffusion barrier resulting in the reduced intermixing (miscibility) and subsequent weakening of the joint [75]. Dislocation movement and diffusion can be improved by increasing the applied pressure beyond ~102 MPa [72]. On the other hand, base metal strength of copper is degraded due to recrystallization during HIP. Additionally, it was observed that the tensile strength decreases with an increase in the tensile testing temperature. However, the strength of solid-form Cu–15%Al/SS joints exactly match the structural requirement of ITER [122]. The report lacks the discussion on the microstructural evolution for Cu–15%Al/SS joints [83]. Interestingly, for the solid-form Cu–25%Al/SS, powder-form Cu–25%Al/SS and solid-form Cu–15%Al/SS, similar voids (see Figure 6a) were reported near the interfaces. The reason for the voids is precipitation of Fe–Cr–B precipitate. Despite this fact, there is a significant difference in the tensile strength. Interestingly, Cu–Ni–Be/SS does not report any voids, but the tensile strength is lower than Cu–15%Al/SS joint. In contrast, the void formation near the interface is found elsewhere while processing the dissimilar joints of Cu–Ni–Be/SS [76]. The details of the mechanism of void formation were discussed; however, the authors did not provide a proper explanation to correlate the joints' tensile property and microstructure. Undoubtedly, the shear strength is higher over the temperature range of 25–400 °C for the Cu–Ni–Be/SS joints compared to the Cu-15%Al/SS and Cu-25%Al/SS joints. However, the room-temperature shear strength of the Cu–Ni–Be/SS and Cu–15%Al/SS is similar. The present situation may be attributed to the differences in the base material composition and plate presence as in the case of Ni–Be precipitation. Morphological alteration in Ni–Be precipitation contributed to tensile property degradation attributed to the joint's cooling cycle (see Figure 6b) [83].
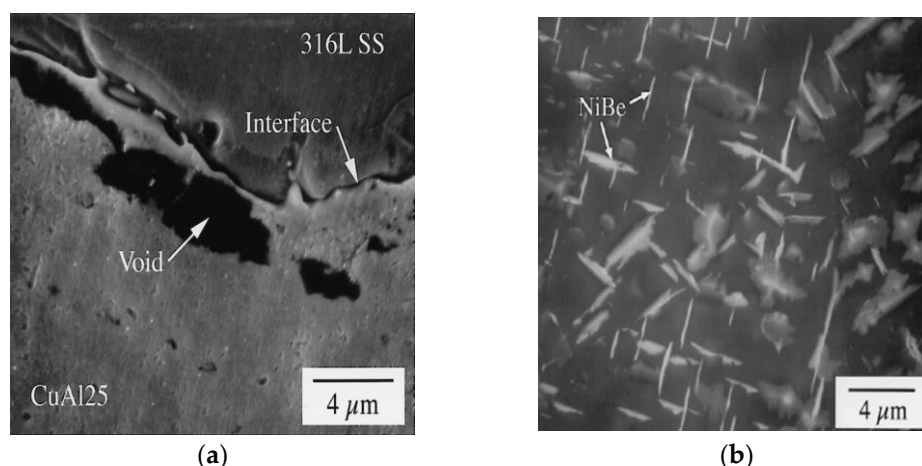
**Figure 6.** (**a**) Micro voids and (**b**) NiBe precipitation while HIP of Cu/SS joints. Reprinted from Ref. [83]. Copyright © 2022 by Elsevier.

Extensive investigation on Cu/SS bimetallic joints by HIP has been carried out to date, as mentioned in the previous paragraph. The work has been attempted mainly to fulfil the joints' requirement for applications in ITER [82,91]. From the above conditions explored by different researchers, it is realized that the optimum process condition is 1050 °C, 150-MPa pressure and two hours' holding time. Post heat treatment is not advisable to achieve the desired property requirements prescribed for ITER. On trying the other possibility, both processing temperature and pressure are brought down [127] using nickel interlayer along with the post-heat treatment to enhance atomic diffusion near the interfacial region. However, optimization of post heat-treatment conditions and the thickness of the intermediate layer need further thorough investigation.

HIP process demands a longer duration time, limited joint geometry, heavy equipment, and a repetitive heating and cooling cycle. Researchers have attempted to investigate the detailed effect of the process parameters on various mechanical and metallurgical properties to develop in-depth knowledge of joint integrity; they found that both understanding of the joint formation and its correlation with process conditions are more complex; however, the application of buffer interlayer in processing Cu/SS joints is not found much in detail. The results obtained for HIP of Cu/SS joint are well accepted as per the requirements of ITER applications; hence, HIP is an excellent candidate for consideration to create the Cu/SS bimetallic joints for an ITER.

*2.2. Diffusion Bonding for Copper/Stainless Steel Bimetallic Joint*

Unlike the conventional HIP equipment and process, diffusion bonding (DB) reports better joint properties at a lower cost [84–87,155]. DB can reduce the cost by 40% compared to the traditional HIP [85]. Table 2 highlights the comparative analysis [84,85] between HIP and DB. The entire process is divided into identifying the optimum interlayer material, bond pressure, process temperature, and bonding duration. In comparison with HIP, it is very much clear that the DB needs significantly reduced holding time and bonding pressure, which results in a cost reduction in processing of the joints. Research [89] has shown that the diffusion phenomenon can be significantly increased along the welded interfaces by using additional electrical current supply in a conventional DB procedure. The electric current supply increases the flow of electrons, which directly influences the atomic-diffusion length. The results of electron dispersive spectroscopy (EDS) confirm the higher distribution of atomic species using additional electric current as compared to a conventional DB method. The study of micro-hardness provides evidence that the external current affects the length of diffusion and quantity, but there is no evidence of change in microstructural morphology. The electrical current induces (indirect) heat into the materials and reduces the dislocation movement across the boundaries, resulting in higher rate of

diffusion in the materials. A direct correlation exists between the atomic-diffusion length and the tensile properties.

**Table 2.** Summary of literature on DB of Cu/SS bimetallic joint.

| Substrate | Thickness (mm) | Joint Design | Parameters | Testing Method | Maximum Obtained Properties of the Joint | Reference |
|---|---|---|---|---|---|---|
| Cu/SS | 10 | P e joint | Fixed parameter<br>Shielding gas: Ar<br>Temperature (°C): 875<br>Heating & cooling rate (°C/min);- 20<br>Pressure (MPa): 3<br>Holding time (h): 2<br>Bonding time (min): 30<br>Type 1<br>Electrical current (A): 5<br>Type 2<br>No electrical current was used | Tensile test<br>Microhardness<br>SEM<br>EDS | UTS (MPa): 170<br>VHN: 240 Hv<br>Optimum condition<br>Type 1 | [95] |
| Cu/410 SS | 3/10 | Butt | Temperature (°C); 800, 850, 900, 950<br>Pressure (MPa): 12<br>Holding time (h): 1<br>Heating (°C/min): 30<br>Ni interlayer: 100 μm | Share strength test<br>Microstructure<br>SEM<br>EDS<br>XRD<br>Microhardness | Share strength (MPa): 145<br>VHN: 432 Hv<br>Optimum temperature 900 °C | [72,96] |
| DS Cu/316 SS | 20 | Butt | Joint type 1<br>Temperature (K); 1123Interlayer material: Au<br>Interlayer thickness (μm); 20, 60<br>Bonding pressure (MPa): 4.8, 9.8<br>Pressed time (h) 1, 2, 3<br>Holding time (h): 1, 2, 3, 4<br>Joint type 2<br>Temperature (K); 1223Interlayer material: Cu<br>Interlayer thickness (μm); 20<br>Bonding pressure (MPa): 4.8, 9.8<br>Pressed time (ks) 0.2, 1.4<br>Holding time (h): 1<br>Joint type 3<br>Temperature (K): 1223Interlayer material: Ni<br>Interlayer thickness (μm); 20<br>Bonding pressure (MPa): 4.8, 9.8<br>Pressed time (ks) 0.3, 1, 1.1<br>Holding time (ks): 3.6, 7.2 | Microstructure<br>Tensile test<br>Charpy impact test | UTS (MPa): 420<br>Charpy absorbed energy (J): 25<br>Optimum condition<br>Temperature (K); 1123Interlayer material: Au<br>Interlayer thickness (μm); 20<br>Bonding pressure (MPa): 4.8<br>Pressed time (ks) 3.6<br>Holding time (ks): 3.6 | [154] |
| Cu/SS | 100 | Butt | Interlayer: Au (5 μm) + Tin-bronze (500 μm), Tin-bronze (100 μm), Au (100 μm)<br>Temperature (°C); 830, 850, 920, 950<br>Bonding pressure (MPa): 3<br>Pressed time (min): 60 | Tensile test<br>Microstructure<br>SEM<br>EDS | UTS (MPa): 228 at 0.5 mm/min strain rate<br>Optimum condition<br>Interlayer: Au (5 μm) + Tin-bronze (500 μm)<br>Temperature (°C); 850 | [98] |
| ETP Cu/AIAI 304 SS | 20 | Butt | Temperature (°C); 700–925<br>Bonding pressure (MPa): up to 12<br>Pressed time (min): up to 30<br>Shielding gas: Ar at 3 bar | Microstructure<br>SEMEDS<br>XRD | Optimum condition<br>Temperature (°C); 800–850<br>Bonding pressure (MPa): 4–6.5<br>Pressed time (min): 15–20 | [92] |
| Cu/304 L SS | 12 | Butt | Interlayer: Ni (0, 12.5, 50 μm)<br>Temperature (°C); 825, 850, 875<br>Bonding pressure (MPa): 5–20<br>Pressed time (min): 5, 10, 20 | Tensile test<br>Microstructure<br>SEM<br>EDS | UTS: (Mpa): 217<br>Optimum condition<br>Temperature (°C); 850<br>Bonding pressure (MPa): 5–20<br>Pressed time (min): 20<br>Interlayer thickness (μm): 15 | [93] |

**Table 2.** *Cont.*

| Substrate | Thickness (mm) | Joint Design | Parameters | Testing Method | Maximum Obtained Properties of the Joint | Reference |
|---|---|---|---|---|---|---|
| ETP Cu/ AISI 304 SS | 20 | Butt | Temperature (°C); 700, 800, 900 Bonding pressure (MPa): 0.2, 0.65, 1.2 Pressed time (min): 5, 15, 30 Shielding gas; Ar | Tensile test SEM EDS | Specific strength or Joint efficiency (μ): 0.8–1 Optimum condition Temperature (°C); 800–850 Bonding pressure (MPa): 10 Pressed time (min): 20–30 | [99] |

The atomic diffusivity is a function of the temperature [90,156,157]. These studies [90,156,157] reported that the atomic diffusion at Cu/Ni and Ni/SS interfaces increases along with the processing temperature from 800 to 950 °C. The details of Kirkendall voids at both the interfaces are an exact match with those of other published works [83,87,92,155]. The adverse impact of voids on the joints was reported for the joints processed at and above 900 °C. The higher heat energy creates the diffusion gradient, and therefore copper endorses the vacancy adjacent to the interface due to the higher activity of chromium near the region. This leads to the voids. The void significantly appears near the Cu/Ni interface rather than the Ni/SS interface [90,155,156]. The reason is the diffusion gradient. Impulse pressing can reduce the size of the voids [87]. In this context, the optimization of the process parameters can be studied to mitigate or avoid the holes or ultrasonic vibration to enhance atomic diffusion [158]. Undoubtedly, better mechanical properties (see Table 2 [156]) can be achieved by altering the material of interlayer. Furthermore, Au with an Sn-bronze interlayer has also been explored, but the mechanical properties reported were significantly less compared to that of the Au interlayer. The joint efficiency relative to the softer base material for DB of Cu/SS bimetallic joining has been reported [87,89,92,93,155]. Extensive work is demanded in the area to eliminate the voids, increases the mechanical properties at room and elevated temperatures, selection of appropriate interlayer and its thickness, optimum process window in correlation with different joint properties and to improve the electrical resistivity [92]. Nishi et al. [94,95,155,159] carried out extensive work to understand the Cu/SS by DB method.

*2.3. Explosive Welding for Copper/Stainless Steel Bimetallic Joint*

Explosive welding (EW) has been developed for industrial application since the 1940s, and detailed exploration of the process for different material has reviewed since then [96,104]. Furthermore, detailed discussion on the process is published by Livne et al. [104]. Despite the involvement of explosive material, the process has been put to use for joining of different materials [96], wherein localized plastic deformation over a range of area can be obtained. A few research works are available for the joining of bimetallic Cu/SS [96–98,104,125]. The initial study to weld Cu/SS by EW focuses on the joining conditions such as weight ratio $\left( R = \frac{Explosive\ weight}{Flyer\ plate\ weight} \right)$, parallel plate, oblique plate [104]; however, the details on standoff distance are not available in the article. At the same time, the effect of combined standoff distance and R-value is discussed in detail elsewhere [97]. It seems that the work is more inclined towards the impact of R-value on to the joint formation [104]. There is little doubt that the metallographic morphology illustrated away from the detonation point presented dominance of the wavy interface. Furthermore, the degree of intermixing is directly proportional to the weight ratio (R). These results are in conformance with another work published [97]. It was observed that the joints were planar near to the detonation region due to the significant effect of weight ratio (R).

The compositional gradient increases from one wave, defined as molten pockets, to another [104]. The heterogeneous microstructures along the circumference of the molten

pockets were mainly attributed to the cooling rate. The cooling rate at the centre of pocket is relatively slow compared to the circumference. However, the heterogeneity in EW is over the entire limited region of interface. Using the EW route for the dissimilar joints, the researchers achieved a tensile strength of 294–372 MPa. Although the strength of base metals is not discussed anywhere else in the paper, the details on the tensile fracture show that the joints' preferred fracture path was along the copper base metal, which reveals that the dissimilar joints prepared using EW are of far better quality. In addition, it was observed that the mechanical properties increase with standoff-distance and weight-ratio (R) [97] due to the sufficient plastic deformation experienced because of higher impact velocity. The literature [96–101,103,104,125] on EW of Cu/SS highlights that the joints have potential to draw more extensive applications. However, a detailed study is needed to explore the effect of temperature on wide range of properties. It is very well established that EW is an efficient process for joining of the bimetals Cu/SS, despite the challenges faced, such as safety due to the involvement of explosions and the degree of heterogeneity in the molten pockets due to cooling rate

### 2.4. Friction Welding for Copper/Stainless Steel Bimetallic Joint

Researchers have explored friction welding (FW) to join the dissimilar metals, but limited their investigation to pipe joints [160–163]. FW has shown significant potential to join copper with stainless steel [105–108]. Joint integrity mainly depends upon the formation of intermetallic along the interfaces. The radial pressure uses the shorter welding time and the sub-melting temperature which eliminates the formation of intermetallic compounds during FW [105,133,164]; hence, sound joints result. The initial study focused on joining 25-mm thick Cu–Cr–Zr to 316 grade SS [109]; wherein, ~2200 RPM, ~353-MPa frictional pressure for 2 s and ~608-MPa upset pressure for 7 sec were employed and the resultant joint between the dissimilar metals exhibited tensile strength greater than the tensile strength of copper (which is ~544 MPa), although the strain rate is unknown. Hence, it is clear that the FW process resulted favourable joint properties of Cu/SS amalgamation. On the other hand, hardness analysis showed the significant effect of heat along the interfacial region of Cu/SS, and in particular the copper-side of the interfacial region. Hardness analysis also indicated that the fracture propagates through the heat affected zone (HAZ) along the copper base-metal. A similar hardness gradient along both the sides of the interfacial region was reported in some other works published [97,98,100,106–108]. This clearly indicates limited atomic mobility along both sides of the interfaces for FW procedure compared to other solid-state welding processes such as HIP and DB. Interestingly, tensile properties of 25-mm thick Cu/SS joints were similar to the copper base-metal with lower frictional pressure, upset pressure and RPM [107,108]. In contrast, the study on the heat transfer model for FW of copper to steel has been carried out, and the author [105] has employed a high level of RPM and force. However, the welding duration is in line with work published elsewhere [109].

### 2.5. Friction Stir Welding for Copper/Stainless Steel Bimetallic Joint

The techno-economical aspect of the friction stir welding (FSW) process and its advantages draws the attention of researchers towards the FSW for copper/stainless-steel bimetallic joining. Undoubtedly, the Cu/SS bimetallic joint's aforementioned critical applications are also one more reason for the industrial and academic attention towards the FSW process. However, the published works on the same materials are limited [110–112,114–119,165] and summarized in Table 3. Dissimilar material welding via the FSW route needs extra care to obtain sound joints [5,63,166–170]; the reasons are the diversified properties across the joint line [168,169,171] such as melting point, thermal conductivity and coefficient of thermal expansion, flow stress and miscibility (solubility). In addition, the selection of tool material is the most important aspect along with its design, because the joining takes place due to the heat induced (~80%) by tool shoulder [102,103,107–111,161–163] and the tool pin governs the stirring action. In a study [120] on the effect of tool shoulder diameter,

18-mm shoulder-diameter with taper tool-pin geometry found suitable for producing quality joints of Cu/SS by FSW. For materials (such as Al) having lower melting range, tool steel [172–175] is preferred as the tool material. On the other hand, FSW of copper and stainless-steel requires a tool material with a higher melting range, red-hot hardness, and strength; hence, poly-crystalline boron-nitride and tungsten-carbide are preferred to join materials with higher melting points and strength [93,176–179]. However, tool wear is also one of the major challenges, and limited studies are published on this topic [99,118,180–184]. In fact, tool wear can be avoided by adopting cryogenic treatment [185–189] of the tool materials. Both fixtures and backing plates play a key role in heat balance across the cross-section [190] of the joints. Despite a lower processing temperature than the materials' melting point, the heat input (from the tool of FSW) must enable the plastic flow of the base materials across the joint line. The heat within the weld area can be retained for a longer time by the judicious selection of proper material for backing plate and fixture; hence, 304L SS is selected for such an application due to its lower thermal conductivity characteristics. On the other hand, sticking of copper with backing plate can also be addressed in the case of high plunge depth. In this case, the researcher has employed the mica sheet beneath the workpiece [110,111]. Similarly, appropriate plastic deformation can also be obtained by applying heat-assisted FSW for Cu/SS joints [121,191–193]. The additional heat source, i.e., gas tungsten arc welding torch, ahead of the non-consumable rotating tool softens the base-materials [194–197]. Hence, the tool of FSW obtained optimal plastic deformation due to the reduced load on the tool, which eventually leads to improved tool life

**Table 3.** Summary of current achievements on FSW of Cu/SS bimetallic joint.

| Substrate | Thickness (mm) | Joint Design | Parameters | Testing Method | Properties of the Joint | Reference |
|---|---|---|---|---|---|---|
| Cu/316L SS | 5 | Butt | RPM: 720<br>Weld speed (mm/min): 16<br>Tool material: tool shoulder of Mo and pin of WC<br>SD (mm): 22<br>Shielding gas: Ar<br>Tool pin type: Cylindrical<br>Pin Length (mm): 4.9<br>Pin diameter(mm): 5 | Tensile test<br>Microstructure<br>SEM<br>Microhardness | UTS (MPa): 225.6<br>JE (%): 85<br>VHN: 290 Hv | [117] |
| Cu/316L SS | 2 | Butt | RPM: 1000, 1500<br>Weld speed (mm/min): 100, 200, 300, 350, 450, 550<br>Tool pin penetration (SS side) (mm): 0, 0.6, 1.6<br>Tool material: WC-14 Co<br>Shoulder (convex) (mm): 25<br>Pin length (mm): 1.35<br>Maximum pin diameter(mm): 5.5<br>Tool pin type: taper | Tensile test<br>Microstructure<br>Micro hardness | UTS (MPa): 267<br>JE((%): 87<br>VHN: 60–100 Hv<br>Optimum condition<br>RPM: 1000<br>Welding speed (mm/min): 300<br>Tool pin penetration (SS side) (mm): 0 | [116] |
| Cu/304L SS | 3 | Butt | RPM: 1000<br>Tool pin offset (mm): −0.6 (steel side), 0, 0.6, 0.9<br>Welding speed (mm/min) 14–112<br>Tool tilt angle: 1.5°<br>Tool material: WC<br>Tool pin length: NR<br>Tool shoulder diameter (mm): 18<br>Tool pin diameter (mm): root is 5 and t is 3<br>Tool pin type: taper | Tensile test<br>Microstructure<br>Micro hardness | UTS (MPa): 171.3 at 1.5 mm/min strain rate<br>JE (%): 69<br>% EL: 6.8<br>VHN: 300 Hv<br>Optimum condition<br>Welding speed (mm/min): 40<br>Tool pin offset (mm): 0.9 towards Cu side | [118] |

Table 3. *Cont.*

| Substrate | Thickness (mm) | Joint Design | Parameters | Testing Method | Properties of the Joint | Reference |
|---|---|---|---|---|---|---|
| Cu/304L SS | 2 | Butt | RPM: 1000<br>Tool pin offset (mm): 3 (Cu side)<br>Welding speed (mm/min) 40<br>Tool tilt angle: NR<br>Tool material: WC<br>Tool pin length: NR<br>Tool shoulder diameter (mm): 10<br>Tool pin diameter (mm): root is 4 and the t is 2 | Tensile test<br>Microstructure<br>Microhardness | UTS (MPa); 216 at 2 mm/min strain rate<br>VHN: 250 Hv | [164] |
| Cu/304L SS | 3 | Butt | RPM: 700, 760, 950, 1170, 1450<br>Tool pin offset (mm): 1 (SS side)<br>Welding speed (mm/min) 25,31.5,40,50,60<br>Tool tilt angle (°): 1, 1.3, 1.8, 2.3, 2.6<br>Tool material: Shoulder is of M2 tool steel and pin is of WC<br>Tool pin length: 2.5<br>Tool shoulder diameter (mm): 22<br>Tool pin shape: trapezoidal<br>Tool pin diameter (mm): root is 22 and t is 17 | Tensile test<br>Microstructure<br>Micro-hardness<br>SEM-EDS | UTS (MPa): 217.2 at 1 mm/min strain rate<br>JE (%): 79<br>% EL: 20.7<br>VHN: 250<br>Optimum condition<br>RPM: 950<br>Welding speed (mm/min): 40<br>Tool tilt angle(°): 1.8 | [120] |
| Cu/DSS | 4 | Butt | RPM: 1000,1200,1400<br>Tool pin offset (mm) (Cu side): 0,0.5,1<br>Tool plunge depth (mm): 0.1<br>Welding speed (mm/min) 20,30<br>Tool tilt angle (°): 3<br>Tool material: WC<br>Tool pin length (mm): 4<br>Tool shoulder diameter (mm): 20<br>Tool pin diameter (mm): root is 5 and t is 3 | Tensile test<br>Microstructure<br>Micro-hardness<br>SEM-EDS<br>XRD | UTS (MPa): 279 at $1 \times 10^{-3}$ s$^{-1}$ strain rate<br>JE (%): 96<br>VHN: 280<br>Optimum condition<br>RPM: 1200<br>Weld speed (mm/min): 30<br>Tool pin offset (Cu side) (mm): 0.5 | [114,115] |
| CuCrZr/316LSS | 6/3 | Lap | RPM: 850<br>Tool plunge depth (mm): 0.5<br>Welding speed (mm/min) 50<br>Tool tilt angle (°): 2.5<br>Tool material: WC-25 Re<br>Tool pin length (mm): 4<br>Tool shoulder diameter (mm): 16<br>Tool pin shape: taper spiral<br>Tool pin diameter (mm): root is 7.5, and the t is 6 | Tensile test<br>Lap shear testing<br>Microstructure<br>Micro-hardness<br>SEM-EDS<br>XRD | UTS (MPa): 305<br>%El: 50<br>Shear test peak load: 19 KN<br>Shear extension (mm): 1.2 | [121] |
| 110 Cu/316 SS | 6 | Butt | RPM: 400, 500<br>Weld speed (mm/min): 25, 50<br>Tool pin offset (mm): 2 (Cu side)<br>Tool tilt angle (°): 2.5<br>Tool material: W-Re<br>Tool shoulder diameter (mm): 16<br>Tool pin diameter (mm): root is 7 and t is 5<br>Pin length (mm): 4 | Tensile test<br>Microstructure<br>SEM<br>EDX | UTS (MPa): 225<br>JE (%): 100<br>VHN: around 375<br>Optimum condition<br>RPM: 400<br>Weld speed (mm/min); 50 | [122] |
| C71000/304 SS | 2 | Butt | RPM: 800, 1000<br>Weld speed (mm/min): 40, 60, 80<br>Tool pin offset (mm): 0.75 (Cu side)<br>Tool tilt angle (°): 2.5<br>Tool material: WC<br>Tool shoulder diameter (mm): 18<br>Tool pin diameter (mm): 6<br>Tool pin type: Cylindrical<br>Pin length (mm): 1.8 | Tensile test<br>Microstructure<br>SEM<br>EDX<br>XRD | UTS (MPa): 285<br>%El; 21<br>JE (%): 84<br>VHN: around 173 | [119] |

The microstructural results are a clear reflection of the parametric conditions and the tool design. Particles in diversified sizes and shapes are distributed and became part of the welded area. The interaction between tool pin and SS base-metal (workpiece) is limited due to the tool offset towards the copper side [111,115,116,119,165]. One of the prime reasons

for shifting the tool pin towards the copper side is to reduce the load on the tool during processing of the joints, and eventually to increase the tool's reliability [193]. At the same time, heat balance can also be obtained by shifting the tool towards the copper side; in doing so, plastic flow can be increased by higher demand for the high heat input than SS due to the higher thermal conductivity of copper. Apart from this, researchers [112,115,117] have attempted to offset the tool towards the SS side, wherein sound joints, i.e., free of macro and micro defects, were successfully created. This contrasts with the result presented by another group [107] in which porosity and cracks resulted from ferrous participation in the welded region. On the one hand, this is not a generalized case while joint consolidation depends on the other parametric conditions and mainly on the tool pin's material flow. On the other hand, the maximum-sized dispersed particle is identified within the weld area when the tool is shifted towards the stainless-steel side. [112,115,117]. This corresponds to the tool shoulder diameter and tool pin dimensions in conjunction with FSW parameters (refer Table 3).

Defects are more likely at the property damping zone. On the other side, the formation of stainless-steel dispersed particles creates the desired intermixing with copper. The report presented the lack of material filling around the scattered stainless steel particle land up with cavity and therefore degraded the joint properties [115] (see Figure 7). A solution to this problem while shifting the tool towards the SS side is available in thermomechanical modelling [110] research. From the simulation work, the higher stress gradient across the faying surfaces leads to the slipping of the material while moving from the leading side to the trailing side of the joint. It will create a material deficiency to fill-up. Hence, the understanding of dispersed stainless steel particle formation and transportation mechanism is of interest to obtain better joint properties. It appears difficult from the literature review. However, it can be correlated with the heat input and the area of tool pin interaction. The higher heat with limited interaction between the SS base material and tool pin (tool pin offset towards the copper side, i.e., softer material region) affected the dispersed particle's size [110,111,114–116,119]. The dispersed particle's size increases with the high heat input parameter. It is doubtless that the heat input is also responsible for particle dispersion from the SS base material into the welded area. The tool pin shape is also the factor which contributes to the same [114,116].
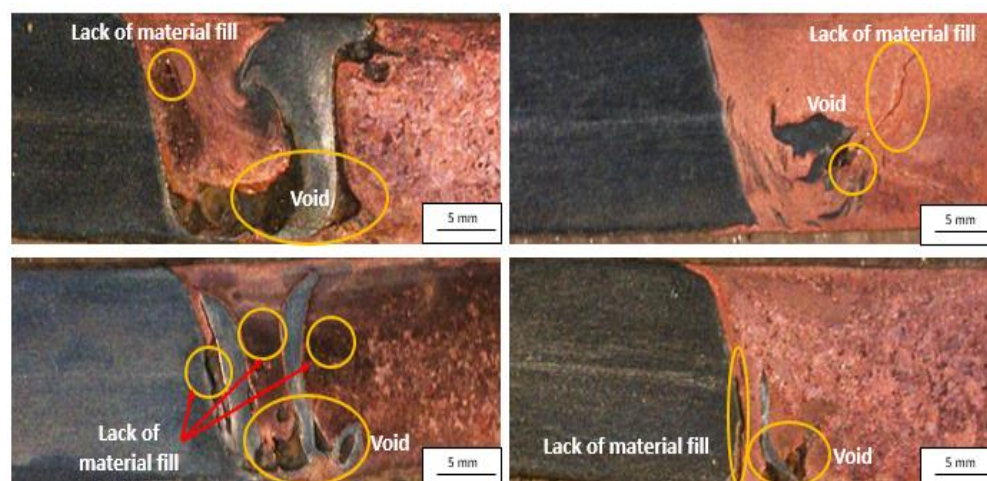


**Figure 7.** Defects of Cu to SS welded samples via FSW. Reprinted from Ref. [125]. Copyright © 2022 by Springer Nature.

In this context, the thermomechanical modelling has been reported, and the flow of plasticized material is discussed [110]. Moreover, the SS dispersed particle will be detached from the base material (stainless steel) and then moved beneath the shoulder, where high temperature is experienced. Subsequently, it pushed towards the pin tip at the lower temperature zone. The pin then rotates it and fills the trailing gap during the tool's forward

traverse. The motion of the particle mentioned above also depends upon the material flow speed. Material flow can be predicted through the contact condition between the tool and the deforming sheet. From the simulation results, it is safe to conclude that the tool pin creates the specific rotation flow zone and can be explained by pseudo-sticking state, i.e., governed by the process temperature. The sticking of dispersed stainless-steel particle enables a pin to move it from the advancing side (AS) and keep it at the joint's trailing side. The discussion is in line with the macro- and microstructure presented elsewhere [110,111,114–119,165]. The movement of stainless-steel [119] dispersed particles can be understood in detail in correlation with the welding temperature. The SS suspended particle is situated very near to that of the SS base material interface in each case. It confirms the efficient sticking phenomenon between the tool and the deformed material, i.e., SS. Interestingly, the size of the particle increases with the increase in the processing temperature. Here, the temperature level is predicted by the set of parameters. The SS deformed particle size increases with the increase in the tool rotation from 400 to 500 RPM for both tool traversing speeds: 25 and 50 mm/min. It suggests that the faster impact with SS base material will tear the smaller parts of the SS base. It is wise to conclude that the dispersed SS particles are either from the base material (primary ones) or smaller SS particles (secondary ones) detached from the larger SS particles. The reported model suggests that the detachment of secondary SS particles depends upon the temperature [110]. Moreover, the detailed work is needed to understand the material flow during FSW of dissimilar materials such as copper and stainless steel.

Similarly, to avoid or to eliminate the stretching of stainless-steel particles within the weld area, researchers [112] have recommended the maximum possible offset towards the copper side, wherein the pin is barely touching the stainless-steel base metal. However, the matter is not whether ferrous particle participation is desirable or avoided because good mechanical properties have been reported during each case (Table 3). The hardness graph of the article published [112] confirms the ferrous participation within the joint. On the other hand, one can compare the hardness profile with the tool pin and the stainless-steel interaction. In some cases, the tensile specimen is fractured from the interfaces or the nugget due to the stress concentration over the welded region [111,116]. The heat input is also reported as one reason for fracture at the interface of the weld and stainless-steel base metal. By reviewing the parametric conditions, the higher heat input is responsible for the fracture from the interface [116]. The energy dispersive x-ray analysis and x-ray diffraction results are also in line with the discussion mentioned above [111,116–119]. Until now, the researcher has exploited the effect of welding speed, RPM, tool pin offset and tool tilt angle on to the joint formation while friction stir welding of Cu/SS (Table 3). Most of the articles reported work on a square butt joint, and the thickness range is 2–6 mm. The lap joint configuration is also exploited [118]. On the other hand, thermomechanical modelling has even been attempted to understand the material distribution and residual stress on the copper/stainless-steel bimetallic joint in FSW [110]. Interestingly, distinct tool shoulder and tool pin material has been applied to weld copper/stainless-steel during FSW [114,117,120,121]. Overall, extensive experimental investigation is needed to know the effect of weld condition on joint formation.

### 2.6. Another Solid-State Welding for Copper/Stainless Steel Bimetallic Joint

Apart from the above discussed solid-state joining processes, ultrasonic spot welding [198] and the electromagnetic impact technique [199] are studied to join copper with stainless steel, wherein the intermixing region of the joint is comparatively less, which can be confirmed through hardness [199] and microstructural [198] analyses. Interestingly, the microstructural feature discussed for ultrasonic welding is similar to the explosive welding (EW) of copper/stainless-steel. In challenges related to the diversified properties, such as thermal conductivity, reflectivity is eliminated. However, the stacking of materials while ultrasonic welding shows a significant effect on mechanical properties [198]. The higher tensile shear failure load is recorded when copper is placed at the side of the

sonotrode. This, in turn, is attributed to the deformation properties of the copper under vibratory conditions. Similarly, the mechanical interlocking is found when copper is joined with stainless-steel by employing the electromagnetic impact technique [199]. However, micro cracks and voids observed in the copper-rich region show evidence of infiltration. Moreover, the articles [198,199] successfully convey the mentioned processes' feasibility for joining copper with stainless steel. However, it is limited to sheet metals. At the same time, extensive experimental work must be carried out in this area.

### 3. Conclusions and Future Work

Herein, the literature has been reviewed to understand better the different joint characteristics of dissimilar metals joints copper/stainless-steel (Cu/SS) by various solid-state welding processes, i.e., diffusion bonding (DB), hot-isostatic pressing (HIP), explosive welding (EW), friction stir processing (FSP), friction stir welding (FSW), and ultrasonic welding (UW). Good joining of copper to stainless-steel has been achieved. Moreover, the present review on the research topic allows the following conclusions:

1. Despite obtaining strong weld joints, both DB and HIP face limitation due to part geometry, longer joint formation time, repetitive heating and cooling cycles, and heavy equipment involvement. However, the DB is cost-effective compared to those of HIP. While DB further increases the quantity and length of material diffusion (copper and stainless steel), the electric current application improves in tensile properties. However, work needs to be done to identify the interlayer material and its thickness while adopting DB and HIP processes to synthesize the dissimilar joints of Cu/SS.

2. The ratio of explosive material weight to flyer plate weight and standoff distance are key parameters during EW of Cu/SS. The mechanical properties of the joint increase with the increase in the above-mentioned factors. The microstructural heterogeneity and the extent of diffusion across the joint interface are considered as limitations. The joint interface experiences plastic deformation due to impact energy. The heterogeneity across the length of the joint and within the molten pocket are the main challenges, along with the risk involved in the explosion. Furthermore, diversified dissimilar joint geometries must be explored to increase the application of EW process to join Cu/SS system.

3. The thin layer of intermetallic compounds along the interface during FSW of Cu/SS, present due to limited diffusion compared to DB and HIP, is the essential characteristic of FSW. The tool pin offset on either side of the joint line is the critical factor in deciding the soundness of the Cu/SS joint in FSW. However, offsetting towards the copper side is recommended. The effects of tool pin geometry and shoulder features are not explored during FSW of Cu/SS. Thermal assistance under FSW decreases the load on tool and enhances the joint's plastic deformation; however, future researchers must establish optimal heat assistance and methods. The material transport mechanism in correlation with the tool interaction with both copper and stainless-steel base materials is of great interest to obtain better joint properties and higher tool life during the FSW of a Cu/SS bimetallic system. While tensile testing, the strain rate has a significant effect on the strength of the joints; hence, strength of the dissimilar joints has to be compared in relation with strain rate of the test.

4. In general, EW, FSW, and UW processes were less explored to join the Cu/SS bimetallic system compared to DB and HIP.

5. Understanding the effect of the geometries (form factor) on the deformation behaviour of both copper and SS are essential to find the optimal operating window for effective and efficient joints of Cu/SS during DB, EW, FSW, HIP, and UW processing routes; hence, a thorough study is targeted on this aspect.

## References

1. Paul, H.; Chulist, R.; Mania, I. Structural Properties of Interfacial Layers in Tantalum to Stainless Steel Clad with Copper Interlayer Produced by Explosive Welding. *Metals* **2020**, *10*, 969. [CrossRef]
2. Lavrishchev, A.V.; Prokopev, S.V.; Tynchenko, V.S.; Myrugin, A.V.; Kukartsev, V.V.; Bashmur, K.A.; Sergienko, R.B.; Tynchenko, V.V.; Lysyannikov, A.V. Investigation of the Solid-Phase Joint of VT-14 Titanium Alloy with 12KH18N10T Stainless Steel Obtained by Diffusion Welding through Intermediate Layers. *Metals* **2021**, *11*, 1325. [CrossRef]
3. Gu, X.; Cui, Z.; Gu, X.; Shao, J. Wire-Feeding Laser Welding of Copper/Stainless Steel Using Different Filler Metals. *Materials* **2021**, *14*, 2122. [CrossRef] [PubMed]
4. Carvalho, G.H.S.F.L.; Galvão, I.; Mendes, R.; Leal, R.M.; Loureiro, A. Aluminum-to-Steel Cladding by Explosive Welding. *Metals* **2020**, *10*, 1062. [CrossRef]
5. Ahmed, M.M.Z.; Ataya, S.; Seleman, M.M.E.-S.; Allam, T.; Alsaleh, N.A.; Ahmed, E. Grain Structure, Crystallographic Texture, and Hardening Behavior of Dissimilar Friction Stir Welded AA5083-O and AA5754-H14. *Metals* **2021**, *11*, 181. [CrossRef]
6. Jairaja, R.; Naik, G.N. Fabrication of Single and Dual Adhesive Bonded Lap Joints Between Dissimilar Composite Adherends. In *Industry 4.0 and Advanced Manufacturing*; Chakrabarti, A., Arora, M., Eds.; Springer: Singapore, 2021; pp. 185–195.
7. Kobayashi, T.; Shohji, I. Fabrication of Three-Dimensional Microstructure Film by Ni-Cu Alloy Electrodeposition for Joining Dissimilar Materials. *Mater. Sci. Forum* **2021**, *1016*, 738–743. [CrossRef]
8. Jambhale, S.; Kumar, S.; Kumar, S. Characterization and Optimization of Flat Friction Stir Spot Welding of Triple Sheet Dissimilar Aluminium Alloy Joints. *Silicon* **2021**, *14*, 815–830. [CrossRef]
9. Beygi, R.; Zarezadeh Mehrizi, M.; Akhavan-Safar, A.; Safaei, S.; Loureiro, A.; da Silva, L.F.M. Design of Friction Stir Welding for Butt Joining of Aluminum to Steel of Dissimilar Thickness: Heat Treatment and Fracture Behavior. *Int. J. Adv. Manuf. Technol.* **2021**, *112*, 1951–1964. [CrossRef]
10. Norwood, D.S.; Schneberger, B.M.; Fuller, K.M.; Brown, K. Prediction of Airframe Thermal Stresses for Hybrid Composite-Metallic Structure. In *AIAA Scitech 2021 Forum*; AIAA SciTech Forum; American Institute of Aeronautics and Astronautics: Reston, Virginia, 2021. [CrossRef]
11. Huang, J.; Zeng, J.; Bai, Y.; Cheng, Z.; Wang, Y.; Zhao, Q.; Liang, D. Effect of Adhesive Layer Properties on the Shear Strength of Single-Lap Structures of Dissimilar Materials Based on the Cohesive Zone Model. *J. Mech. Sci. Technol.* **2021**, *35*, 133–143. [CrossRef]
12. Zhou, H.; Lee, J.; Kang, M.; Kim, H.; Lee, H.; In, J. Bin. All Laser-Based Fabrication of Microchannel Heat Sink. *Mater. Des.* **2022**, *221*, 110968. [CrossRef]
13. Guo, Z.; Pan, Y.; Guo, R.; Fang, Z. Fabrication of Fullerene Decorated by Iron Compound and Its Effect on the Thermal Stability and Flammability for High-Density Polyethylene. *Fire Mater.* **2020**, *44*, 506–515. [CrossRef]
14. Wang, D.; Liu, L.; Deng, G.; Deng, C.; Bai, Y.; Yang, Y.; Wu, W.; Chen, J.; Liu, Y.; Wang, Y.; et al. Recent Progress on Additive Manufacturing of Multi-Material Structures with Laser Powder Bed Fusion. *Virtual Phys. Prototyp.* **2022**, *17*, 329–365. [CrossRef]
15. Rodrigues, T.A.; Bairrão, N.; Farias, F.W.C.; Shamsolhodaei, A.; Shen, J.; Zhou, N.; Maawad, E.; Schell, N.; Santos, T.G.; Oliveira, J.P. Steel-Copper Functionally Graded Material Produced by Twin-Wire and Arc Additive Manufacturing (T-WAAM). *Mater. Des.* **2022**, *213*, 110270. [CrossRef]
16. Selema, A.; Ibrahim, M.N.; Sergeant, P. Metal Additive Manufacturing for Electrical Machines: Technology Review and Latest Advancements. *Energies* **2022**, *15*, 1076. [CrossRef]
17. Sadeghian, A.; Iqbal, N. A Review on Dissimilar Laser Welding of Steel-Copper, Steel-Aluminum, Aluminum-Copper, and Steel-Nickel for Electric Vehicle Battery Manufacturing. *Opt. Laser Technol.* **2022**, *146*, 107595. [CrossRef]

18. Vyas, H.; Mehta, K.P. Effect of Multi Pass Friction Stir Processing on Surface Modification and Properties of Aluminum Alloy 6061. *Key Eng. Mater.* **2019**, *813*, 404–410. [CrossRef]

19. Pravin Tamil Selvan, C.; Kalaiselvan, K.; Dinaharan, I.; Palanivel, R. Assessment of Microstructure and Tensile Behavior of Hot Wire Gas Tungsten Arc Welded Pure Nickel Tubes. *Trans. Indian Inst. Met.* **2021**, *74*, 355–368. [CrossRef]

20. Furuya, H.S.; Yabu, S.; Sato, Y.S.; Kokawa, H.; Pereira, B. Metals Microstructural Control of the Interface Layer for Strength Enhancement of Dissimilar Al/Cu Joints via Ni Addition during TIG Arc Brazing. *Metals* **2021**, *11*, 491. [CrossRef]

21. Dai, J.; Yu, B.; Ruan, Q.; Chu, P.K. Improvement of the Laser-Welded Lap Joint of Dissimilar Mg Alloy and Cu by Incorporation of a Zn Interlayer. *Materials* **2020**, *13*, 2053. [CrossRef]

22. Fukumoto, S.; Inuki, T.; Tsubakino, H.; Okita, K.; Aritoshi, M.; Tomita, T. Evaluation of Friction Weld Interface of Aluminium to Austenitic Stainless Steel Joint. *Mater. Sci. Technol.* **1997**, *13*, 679–686. [CrossRef]

23. AlHazaa, A.; Haneklaus, N. Diffusion Bonding and Transient Liquid Phase (TLP) Bonding of Type 304 and 316 Austenitic Stainless Steel—A Review of Similar and Dissimilar Material Joints. *Metals* **2020**, *10*, 613. [CrossRef]

24. Nam, H.; Park, S.; Chun, E.-J.; Kim, H.; Na, Y.; Kang, N. Laser Dissimilar Weldability of Cast and Rolled CoCrFeMnNi High-Entropy Alloys for Cryogenic Applications. *Sci. Technol. Weld. Join.* **2020**, *25*, 127–134. [CrossRef]

25. Graber, L.; Saeedifard, M.; Mauger, M.J.; Yang, Q.; Park, C.; Niebur, T.; Pamidi, S.V.; Steinhoff, S. Cryogenic Power Electronics at Megawatt-Scale Using a New Type of Press-Pack IGBT. *IOP Conf. Ser. Mater. Sci. Eng.* **2017**, *279*, 012011. [CrossRef]

26. Karthikeyan, M. Effect of Tool Travel Speed on Tensile Strength of Friction Stir Welded Dissimilar Joint of Aluminium AA6061 T6 Alloy and Maraging M250 Steel. *Mater. Res. Express* **2021**, *8*, 026502. [CrossRef]

27. Park, S.; Nam, H.; Na, Y.; Kim, H.; Moon, Y.; Kang, N. Effect of Initial Grain Size on Friction Stir Weldability for Rolled and Cast CoCrFeMnNi High-Entropy Alloys. *Met. Mater. Int.* **2020**, *26*, 641–649. [CrossRef]

28. Joshi, G.R.; Badheka, V.J. Processing of Bimetallic Steel-Copper Joint by Laser Beam Welding. *Mater. Manuf. Process.* **2019**, *34*, 1232–1242. [CrossRef]

29. Joshi, G.R.; Badheka, V.J. Metallographic and Microstructure Analysis of Gas Tungsten Arc-Welded Bimetallic Copper-to-Stainless Steel Joints. *Met. Microstruct. Anal.* **2020**, *9*, 180–193. [CrossRef]

30. Bhogendro Meitei, R.K.; Maji, P.; Samadhiya, A.; Karmakar, R.; Ghosh, S.K.; Saha, S.C. An Experimental Investigation on Joining of Copper and Stainless Steel by Induction Welding Technique. *Int. J. Precis. Eng. Manuf.* **2020**, *21*, 613–621. [CrossRef]

31. Nakao, H.; Nishimoto, A. Pulsed-Electric-Current Bonding of Oxygen-Free Copper and Austenitic Stainless Steel. *Mater. Trans.* **2021**, *62*, 448–452. [CrossRef]

32. Pérez Zapico, E.; Ascari, A.; Dimatteo, V.; Fortunato, A. Laser Dissimilar Welding of Copper and Steel Thin Sheets for Battery Production. *J. Laser Appl.* **2021**, *33*, 012016. [CrossRef]

33. Zheng, C.; Pan, C.; Wang, J.; Zhao, G.; Ji, Z. Mechanical Joining Behavior of Cu–Fe Dissimilar Metallic Foils in Laser Shock Clinching. *Int. J. Adv. Manuf. Technol.* **2020**, *110*, 1001–1014. [CrossRef]

34. Tamang, S.; Aravindan, S. Joining of cu to ss304 by microwave hybrid heating with ni an interlayer. In Proceedings of the 17th International Conference on Microwave and High Frequency Heating, Valencia, Spain, 9–12 September 2019; Universitat Politècnica de València: Valencia, Spain, 2019; pp. 98–104. [CrossRef]

35. Osipovich, K.S.; Astafurova, E.G.; Chumaevskii, A.V.; Kalashnikov, K.N.; Astafurov, S.V.; Maier, G.G.; Melnikov, E.V.; Moskvina, V.A.; Panchenko, M.Y.; Tarasov, S.Y.; et al. Gradient Transition Zone Structure in "Steel–Copper" Sample Produced by Double Wire-Feed Electron Beam Additive Manufacturing. *J. Mater. Sci.* **2020**, *55*, 9258–9272. [CrossRef]

36. Niknamian, S. Investigation of Microstructure and Corrosion Resistance of Dissimilar Welded Joint between 304 Stainless Steel and Pure Copper. *Bp. Int. Res. Exact Sci. J.* **2019**, *1*, 76–82. [CrossRef]

37. Huang, Y.; Zha, Y.; Zhou, X.; Li, X.; Li, W.; Guo, Q.; Chen, W.; Peng, D. Evolution of Interfacial Structure of the Joints between a Tungsten-Copper Composite and Austenitic Stainless Steel. *Mater. Res. Express* **2021**, *8*, 16514. [CrossRef]

38. Singh, G.; Saxena, R.K.; Pandey, S. A Three-Dimensional Thermal Finite Element Analysis of AISI 304 Stainless Steel and Copper Dissimilar Weldment. *AIP Conf. Proc.* **2018**, *1943*, 020032. [CrossRef]

39. Singh, G.; Saxena, R.K.; Pandey, S. Investigating the Effect of Arc Offsetting in AISI 304 Stainless Steel and Copper Welding Using Gas Tungsten Arc Welding. *J. Braz. Soc. Mech. Sci. Eng.* **2021**, *43*, 174. [CrossRef]

40. Phanikumar, G.; Manjini, S.; Dutta, P.; Chattopadhyay, K.; Mazumder, J. Characterization of a Continuous CO2 Laser-Welded Fe-Cu Dissimilar Couple. *Met. Mater. Trans. A* **2005**, *36*, 2137–2147. [CrossRef]

41. Tosto, S.; Nenci, F.; Jiandong, H.; Corniani, G.; Pierdominici, F. Microstructure of Copper–AISI Type 304L Electron Beam Welded Alloy. *Mater. Sci. Technol.* **2003**, *19*, 519–522. [CrossRef]

42. Turna, M.; Sahul, M.; Ondruska, J.; Lokaj, J. Electron Beam Welding of Copper to Stainless Steel. In *Annals of DAAAM and Proceedings of the International DAAAM Symposium*; Katalinic, B., Ed.; DAAAM International: Vienna, Austria, 2011; Volume 22, pp. 833–834.

43. Liu, H.W.; Huang, L.; Guo, X.; Lv, Y.L. Residual Stress Analysis of TIG Welding Process of Thin-Walled Stainless Steel and Red Copper. *Adv. Mater. Res.* **2013**, *834–836*, 1553–1556. [CrossRef]

44. Chang, C.C.; Wu, L.H.; Shueh, C.; Chan, C.K.; Shen, I.C.; Kuan, C.K. Evaluation of Microstructure and Mechanical Properties of Dissimilar Welding of Copper Alloy and Stainless Steel. *Int. J. Adv. Manuf. Technol.* **2017**, *91*, 2217–2224. [CrossRef]

45. Rafiei, M.; Mostaan, H. The Effect of Filler Metal and Butter Layer on Microstructural and Mechanical Properties of Pure Cu to AISI304 Stainless Steel Dissimilar Joint. *Proc. Inst. Mech. Eng. Part L J. Mater. Des. Appl.* **2018**, *233*, 1894–1905. [CrossRef]

46. Sahul, M.; Sahul, M.; Turňa, M.; Zacková, P. Disk Laser Welding of Copper to Stainless Steel. *Adv. Mater. Res.* **2014**, *1077*, 76–81. [CrossRef]

47. Chen, S.; Huang, J.; Xia, J.; Zhang, H.; Zhao, X. Microstructural Characteristics of a Stainless Steel/Copper Dissimilar Joint Made by Laser Welding. *Met. Mater. Trans. A Phys. Met. Mater. Sci.* **2013**, *44*, 3690–3696. [CrossRef]

48. Nam, S.; Kim, C.; Kim, Y.-M. Hot Cracking of Ni-Cr-Fe Alloys: Test Methods and Metallurgical Effect. *J. Weld. Join.* **2017**, *35*, 7–15. [CrossRef]

49. Kobatake, H.; Brillo, J. Density and Viscosity of Ternary Cr–Fe–Ni Liquid Alloys. *J. Mater. Sci.* **2013**, *48*, 6818–6824. [CrossRef]

50. Brooks, R.; Egry, I.; Seetharaman, S.; Grant, D. Reliable Data for High-Temperature Viscosity and Surface Tension: Results from a European Project. *High Temp. Press.* **2001**, *33*, 631–637. [CrossRef]

51. Ao, S.S.; Zhang, W.; Li, C.J.; Oliveira, J.P.; Zeng, Z.; Luo, Z. Variable-Parameter NiTi Ultrasonic Spot Welding with Cu Interlayer. *Mater. Manuf. Process.* **2020**, *36*, 599–607. [CrossRef]

52. Sanga, B.; Wattal, R.; Nagesh, D.S. Mechanism of Joint Formation and Characteristics of Interface in Ultrasonic Welding: Literature Review. *Period. Eng. Nat. Sci.* **2018**, *6*, 107. [CrossRef]

53. Shahid, M.B.; Han, S.-C.; Jun, T.-S.; Park, D.-S. Effect of Process Parameters on the Joint Strength in Ultrasonic Welding of Cu and Ni Foils. *Mater. Manuf. Process.* **2019**, *34*, 1217–1224. [CrossRef]

54. Iqbal, N.; Nath, S.; Coleman, A.E.; Lawrence, J. Parametric Study of Pulse Arc Welding (PAW) and Laser Beam Welding (LBW) Techniques for Electrical Vehicle Battery Cells. *Mater. Sci. Forum* **2021**, *1016*, 611–617. [CrossRef]

55. Shi, R.P.; Wang, C.P.; Wheeler, D.; Liu, X.J.; Wang, Y. Formation Mechanisms of Self-Organized Core/Shell and Core/Shell/Corona Microstructures in Liquid Droplets of Immiscible Alloys. *Acta Mater.* **2013**, *61*, 1229–1243. [CrossRef]

56. Ma, C.; Chen, B.; Tan, C.; Song, X.; Feng, J. Characteristics of Droplet Transfer, Molten Pool Formation, and Weld Bead Formation of Oscillating Laser Hot-Wire Tungsten Inert Gas Hybrid Welding. *J. Laser Appl.* **2021**, *33*, 012027. [CrossRef]

57. Anbarasan, N.; Narein, N.; Jerome, S. Influence of Mechanical Arc Oscillation on the Microstructural and Mechanical Properties of Inconel 718 Welds. *Trans. Indian Inst. Met.* **2019**, *72*, 1541–1544. [CrossRef]

58. Wang, J.; Sun, Q.; Feng, J.; Wang, S.; Zhao, H. Characteristics of Welding and Arc Pressure in TIG Narrow Gap Welding Using Novel Magnetic Arc Oscillation. *Int. J. Adv. Manuf. Technol.* **2017**, *90*, 413–420. [CrossRef]

59. Dinda, S.K.; Das, D.; Mohan, A.; Srirangam, P.; Roy, G.G. Effect of Beam Oscillation on Electron Beam Butt Welded Dual-Phase (DP600) Steel to 5754 Aluminum Alloy Joints. *Metall. Mater. Trans. A* **2021**, *52*, 1723–1731. [CrossRef]

60. Lara, M.; Díaz, V.V.; Camus, M.; Da Cunha, T.V. Effect of Transverse Arc Oscillation on Morphology, Dilution and Microstructural Aspects of Weld Beads Produced with Short-Circuiting Transfer in GMAW. *J. Braz. Soc. Mech. Sci. Eng.* **2020**, *42*, 449. [CrossRef]

61. Karthikeyan, R. Establishing Relationship between Optimised Friction Stir Spot Welding Process Parameters and Strength of Aluminium Alloys. *Adv. Mater. Process. Technol.* **2021**, 1–23. [CrossRef]

62. Zhang, S.; Lueg-Althoff, J.; Hahn, M.; Tekkaya, A.E.; Kinsey, B. Effect of Process Parameters on Wavy Interfacial Morphology During Magnetic Pulse Welding. *J. Manuf. Sci. Eng.* **2021**, *143*, 011010. [CrossRef]

63. Das, H.; Upadhyay, P.; Wang, T.; Gwalani, B.; Ma, X. Interfacial Reaction during Friction Stir Assisted Scribe Welding of Immiscible Fe and Mg Alloy System. *Sci. Rep.* **2021**, *11*, 1588. [CrossRef] [PubMed]

64. Patel, N.P.; Parlikar, P.; Singh Dhari, R.; Mehta, K.; Pandya, M. Numerical Modelling on Cooling Assisted Friction Stir Welding of Dissimilar Al-Cu Joint. *J. Manuf. Process.* **2019**, *47*, 98–109. [CrossRef]

65. Zhang, W.; Ao, S.S.; Oliveira, J.P.; Zeng, Z.; Luo, Z.; Hao, Z.Z. Effect of Ultrasonic Spot Welding on the Mechanical Behaviour of NiTi Shape Memory Alloys. *Smart Mater. Struct.* **2018**, *27*, 085020. [CrossRef]

66. Zens, A.; Zaeh, M.F.; Marstatt, R.; Haider, F. Friction Stir Welding of Dissimilar Metal Joints. *Materwiss. Werksttech.* **2019**, *50*, 949–957. [CrossRef]

67. Bevilacqua, M.; Ciarapica, F.; Forcellese, A.; Simoncini, M. Comparison among the Environmental Impact of Solid State and Fusion Welding Processes in Joining an Aluminium Alloy. *Proc. Inst. Mech. Eng. Part B J. Eng. Manuf.* **2020**, *234*, 140–156. [CrossRef]

68. Kumar, N.; Yuan, W.; Mishra, R.S. Introduction. In *Friction Stir Welding of Dissimilar Alloys and Materials*; Elsevier: Amsterdam, The Netherlands, 2015; pp. 1–13. [CrossRef]

69. Bertinelli, F.; Favre, G.; Ferreira, L.M.A.; Mathot, S.; Rossi, L.; Savary, F.; Boter, E. Design and Fabrication of Superfluid Helium Heat Exchnager Tubes for the LHC Superconductor Magnets. In Proceedings of the EPAC, Lucerne, Switzerland, 5–9 July 2004; pp. 1837–1839.

70. Elio, F.; Ioki, K.; Yamada, M.; Strebkov, Y.; Daenner, W.; Akiba, M. Design and R&D Progress of Blanket Attachments. *Fusion Eng. Des.* **2003**, *69*, 321–326. [CrossRef]

71. Stubbins, J.F.; Kurath, P.; Drockelman, D.; Morgan, G.D.; McAfee, J.; Li, G.; Thomas, B.G. Analysis of Copper Alloy to Stainless Steel Bonded Panels for ITER First Wall Applications. In Proceedings of the 16th International Symposium on Fusion Engineering, 6 August 2002; IEEE: Piscataway, NJ, USA, 2002; Volume 1, pp. 174–177. [CrossRef]

72. Sato, S.; Kuroda, T.; Hatano, T.; Furuya, K.; Tokami, I.; Takatsu, H. Development of First Wall/Blanket Structure by Hot Isostatic Pressing (HIP) in the JAERI. *Fusion Eng. Des.* **1998**, *39–40*, 609–614. [CrossRef]

73. Fabritsiev, S.A.; Pokrovsky, A.S.; Edwards, D.J.; Zinkle, S.J.; Rowcliffe, A.F. Effect of Neutron Irradiation on the Mechanical Properties and Fracture Mode of Cu/Ss Joints. *Plasma Devices Oper.* **2001**, *8*, 225–239. [CrossRef]

74. Le Marois, G.; Burlet, H.; Solomon, R.; Marini, B.; Gentzbittel, J.; Briottet, L. Structural Materials Joints for ITER In-Vessel Components. *Fusion Eng. Des.* **1998**, *39–40*, 253–261. [CrossRef]

75. Le Marois, G.; Dellis, C.; Gentzbittel, J.M.; Moret, F. HIP'ing of Copper Alloys to Stainless Steel. *J. Nucl. Mater.* **1996**, *233–237*, 927–931. [CrossRef]

76. Xu, Q.; Yoshiie, T.; Muroga, T.; Yoshida, N.; Iwai, T.; Edwards, D. Microstructural Evolution and Hardness Changes in the Interface of Cu/316L Joint Materials under Aging and Ion Irradiation. *J. Nucl. Mater.* **2004**, *329–333*, 1558–1562. [CrossRef]

77. Park, J.-Y.; Choi, B.-K.; Kim, H.-G.; Kim, J.-H.; Lee, M.-H.; Park, S.-Y.; Hong, B.G.; Jeong, Y.H. Optimization of Joining Condition for ITER First Wall Fabrication. *J. Korean Phys. Soc.* **2006**, *49* (Suppl. 1), 442–446.

78. Park, J.-Y.; Choi, B.-K.; Lee, J.-S.; Lee, D.W.; Hong, B.G.; Jeong, Y.H. Fabrication of Be/CuCrZr/SS Mock-Ups for ITER First Wall. *Fusion Eng. Des.* **2009**, *84*, 1468–1471. [CrossRef]

79. Tähtinen, S.; Laukkanen, A.; Singh, B. Investigations of Copper to Stainless Steel Joints. *Fusion Eng. Des.* **2001**, *56–57*, 391–396. [CrossRef]

80. Daenner, W.; Merola, M.; Lorenzetto, P.; Peacock, A.; Bobin-Vastra, I.; Briottet, L.; Bucci, P.; Conchon, D.; Erskine, A.; Escourbiac, F.; et al. Status of Fabrication Development for Plasma Facing Components in the EU. *Fusion Eng. Des.* **2002**, *61–62*, 61–70. [CrossRef]

81. Elio, F.; Ioki, K.; Barabaschi, P.; Bruno, L.; Cardella, A.; Hechler, M.; Kodama, T.; Lodato, A.; Loesser, D.; Lousteau, D.; et al. Engineering Design of the ITER Blanket and Relevant Research and Development Results. *Fusion Eng. Des.* **1999**, *46*, 159–175. [CrossRef]

82. Elangovan, K.; Balasubramanian, V. Influences of Tool Pin Profile and Welding Speed on the Formation of Friction Stir Processing Zone in AA2219 Aluminium Alloy. *J. Mater. Process. Technol.* **2008**, *200*, 163–175. [CrossRef]

83. Leedy, K.; Stubbins, J. Copper Alloy–Stainless Steel Bonded Laminates for Fusion Reactor Applications: Tensile Strength and Microstructure. *Mater. Sci. Eng. A* **2001**, *297*, 10–18. [CrossRef]

84. Spence, P.J.; Hall, F.R.; Emekwuru, N. Preliminary Study of Improving the Speed and Cost of Diffusion Bonding of Metal Sheets. *Proc. Inst. Mech. Eng. Part B J. Eng. Manuf.* **2014**, *228*, 95–110. [CrossRef]

85. Testani, C.; Ferraro, F.; Deodati, P.; Donnini, R.; Montanari, R.; Kaciulis, S.; Mezzi, A. Comparison between Roll Diffusion Bonding and Hot Isostatic Pressing Production Processes of Ti6Al4V-SiC$_f$ Metal Matrix Composites. *Mater. Sci. Forum* **2011**, *678*, 145–154. [CrossRef]

86. Yilmaz, O.; Çelik, H. Electrical and Thermal Properties of the Interface at Diffusion-Bonded and Soldered 304 Stainless Steel and Copper Bimetal. *J. Mater. Process. Technol.* **2003**, *141*, 67–76. [CrossRef]

87. Yuan, X.; Tang, K.; Deng, Y.; Luo, J.; Sheng, G. Impulse Pressuring Diffusion Bonding of a Copper Alloy to a Stainless Steel with/without a Pure Nickel Interlayer. *Mater. Des.* **2013**, *52*, 359–366. [CrossRef]

88. Nishi, H.; Kikuchi, K. Influence of Brazing Conditions on the Strength of Brazed Joints of Alumina Dispersion-Strengthened Copper to 316 Stainless Steel. *J. Nucl. Mater.* **1998**, *258–263*, 281–288. [CrossRef]

89. Kaya, Y.; Kahraman, N.; Durgutlu, A.; Gülenç, B. A Novel Approach to Diffusion Bonding of Copper to Stainless Steel. *Proc. Inst. Mech. Eng. Part B J. Eng. Manuf.* **2012**, *226*, 478–484. [CrossRef]

90. Sabetghadam, H.; Zarei Hanzaki, A.; Araee, A.; Hadian, A. Microstructural Evaluation of 410 SS/Cu Diffusion-Bonded Joint. *J. Mater. Sci. Technol.* **2010**, *26*, 163–169. [CrossRef]

91. Lorenzetto, P.; Peacock, A.; Bobin-Vastra, I.; Briottet, L.; Bucci, P.; Dell'Orco, G.; Ioki, K.; Roedig, M.; Sherlock, P. EU R&D on the ITER First Wall. *Fusion Eng. Des.* **2006**, *81 A*, 355–360. [CrossRef]

92. Yilmaz, O.; Aksoy, M. Investigation of Micro-Crack Occurrence Conditions in Diffusion Bonded Cu-304 Stainless Steel Couple. *J. Mater. Process. Technol.* **2002**, *121*, 136–142. [CrossRef]

93. Xiong, J.T.; Xie, Q.; Li, J.L.; Zhang, F.S.; Huang, W.D. Diffusion Bonding of Stainless Steel to Copper with Tin Bronze and Gold Interlayers. *J. Mater. Eng. Perform.* **2012**, *21*, 33–37. [CrossRef]

94. Nishi, H.; Araki, T. Low Cycle Fatigue Strength of Diffusion Bonded Joints of Alumina Dispersion-Strengthened Copper to Stainless Steel. *J. Nucl. Mater.* **2000**, *283–287*, 1234–1237. [CrossRef]

95. Nishi, H. Notch Toughness Evaluation of Diffusion-Bonded Joint of Alumina Dispersion-Strengthened Copper to Stainless Steel. *Fusion Eng. Des.* **2006**, *81 A*, 269–274. [CrossRef]

96. Findik, F. Recent Developments in Explosive Welding. *Mater. Des.* **2011**, *32*, 1081–1093. [CrossRef]

97. Durgutlu, A.; Gülenç, B.; Findik, F. Examination of Copper/Stainless Steel Joints Formed by Explosive Welding. *Mater. Des.* **2005**, *26*, 497–507. [CrossRef]

98. Honarpisheh, M.; Haddadi, A.A.; Mansouri, H. The Effect of Annealing Heat Treatment on the Bond of Explosive—Welded Copper/Steel after the ECAR Process. *J. Mod. Process. Manuf. Prod.* **2018**, *6*, 77–86.

99. Ma, R.; Wang, Y.; Wu, J.; Duan, M. Explosive Welding Method for Manufacturing ITER-Grade 316L(N)/CuCrZr Hollow Structural Member. *Fusion Eng. Des.* **2014**, *89*, 3117–3124. [CrossRef]

100. Durgutlu, A.; Okuyucu, H.; Gulenc, B. Investigation of Effect of the Stand-off Distance on Interface Characteristics of Explosively Welded Copper and Stainless Steel. *Mater. Des.* **2008**, *29*, 1480–1484. [CrossRef]

101. Yang, M.; Ma, H.; Shen, Z.; Sun, Y. Study on Explosive Welding for Manufacturing Meshing Bonding Interface of CuCrZr to 316L Stainless Steel. *Fusion Eng. Des.* **2019**, *143*, 106–114. [CrossRef]

102. Lorenzetto, P.; Boireau, B.; Boudot, C.; Bucci, P.; Furmanek, A.; Ioki, K.; Liimatainen, J.; Peacock, A.; Sherlock, P.; Tähtinen, S. Manufacture of Blanket Shield Modules for ITER. *Fusion Eng. Des.* **2005**, *75–79*, 291–296. [CrossRef]

103. Wang, P.; Chen, J.; Li, Q.; Liu, D.; Huang, P.; Jin, F.; Zhou, Y.; Yang, B. Study on the Microstructure and Properties Evolution of CuCrZr/316LN-IG Explosion Bonding for ITER First Wall Components. *Fusion Eng. Des.* **2017**, *124*, 1135–1139. [CrossRef]

104. Livne, Z.; Munitz, A. Characterization of Explosively Bonded Iron and Copper Plates. *J. Mater. Sci.* **1987**, *22*, 1495–1500. [CrossRef]

105. Sahin, A.Z.; Yibaş, B.S.; Ahmed, M.; Nickel, J. Analysis of the Friction Welding Process in Relation to the Welding of Copper and Steel Bars. *J. Mater. Process. Technol.* **1998**, *82*, 127–136. [CrossRef]

106. Sahin, M. Joining of Stainless Steel and Copper Materials with Friction Welding. *Ind. Lubr. Tribol.* **2009**, *61*, 319–324. [CrossRef]

107. Chinnakannan, S. Friction Welding of Austenitic Stainless Steel with Copper Material. In *Austenitic Stainless Steels—New Aspects*; InTech: London, UK, 2017. [CrossRef]

108. Shanjeevi, C.; Arputhabalan, J.J.; Dutta, R. Pradeep. Investigation on the Effect of Friction Welding Parameters on Impact Strength in Dissimilar Joints. *IOP Conf. Ser. Mater. Sci. Eng.* **2017**, *197*, 012069. [CrossRef]

109. Tsuchiya, K.; Kawamura, H. Mechanical Properties of CuCrZr Alloy and SS316 Joints Fabricated by Friction Welding Method. *J. Nucl. Mater.* **1996**, *233–237*, 913–917. [CrossRef]

110. Shokri, V.; Sadeghi, A.; Sadeghi, M.H. Thermomechanical Modeling of Friction Stir Welding in a Cu-DSS Dissimilar Joint. *J. Manuf. Process.* **2018**, *31*, 46–55. [CrossRef]

111. Shokri, V.; Sadeghi, A.; Sadeghi, M.H. Effect of Friction Stir Welding Parameters on Microstructure and Mechanical Properties of DSS–Cu Joints. *Mater. Sci. Eng. A* **2017**, *693*, 111–120. [CrossRef]

112. Ramirez, A.J.; Benati, D.M.; Fals, H.C. Effect of Tool Offset On Dissimilar Cu-AISI 316 Stainless Steel Friction Stir Welding. In Proceedings of the 21st International Offshore and Polar Engineering Conference, Maui, Hawaii, USA, 19–24 June 2011; Volume 8, pp. 548–551.

113. Akella, M.S.; Harinadh, M.V.; Krishna, M.Y.; Buddu, M.R.K. A Welding Simulation of Dissimilar Materials SS304 and Copper. *Procedia Mater. Sci.* **2014**, *5*, 2440–2449. [CrossRef]

114. Najafkhani, A.; Zangeneh-Madar, K.; Abbaszadeh, H. Evaluation of Microstructure and Mechanical Properties of Friction Stir Welded Copper/316L Stainless Steel Dissimilar Metals. *Int. J. ISSI* **2010**, *7*, 21–25.

115. Imani, Y.; Givi, M.K.B.; Guillot, M. Improving Friction Stir Welding between Copper and 304L Stainless Steel. *Adv. Mater. Res.* **2011**, *409*, 263–268. [CrossRef]

116. Aval, H.J. Microstructural Evolution and Mechanical Properties of Friction Stir-Welded C71000 Copper–Nickel Alloy and 304 Austenitic Stainless Steel. *Int. J. Miner. Metall. Mater.* **2018**, *25*, 1294–1303. [CrossRef]

117. Jafari, M.; Abbasi, M.; Poursina, D.; Gheysarian, A.; Bagheri, B. Microstructures and Mechanical Properties of Friction Stir Welded Dissimilar Steel-Copper Joints. *J. Mech. Sci. Technol.* **2017**, *31*, 1135–1142. [CrossRef]

118. Sahlot, P.; Nene, S.S.; Frank, M.; Mishra, R.S.; Arora, A. Towards Attaining Dissimilar Lap Joint of CuCrZr Alloy and 316L Stainless Steel Using Friction Stir Welding. *Sci. Technol. Weld. Join.* **2018**, *23*, 715–720. [CrossRef]

119. Wang, T.; Shukla, S.; Nene, S.S.; Frank, M.; Wheeler, R.W.; Mishra, R.S. Towards Obtaining Sound Butt Joint Between Metallurgically Immiscible Pure Cu and Stainless Steel Through Friction Stir Welding. *Metall. Mater. Trans. A* **2018**, *49*, 2578–2582. [CrossRef]

120. Joshi, G.R.; Badheka, V.J. Studies on Tool Shoulder Diameter of Dissimilar Friction Stir Welding Copper to Stainless Steel. *Metallogr. Microstruct. Anal.* **2019**, *8*, 263–274. [CrossRef]

121. Joshi, G.R.; Badheka, V.J. Microstructures and Properties of Copper to Stainless Steel Joints by Hybrid FSW. *Metallogr. Microstruct. Anal.* **2017**, *6*, 470–480. [CrossRef]

122. Wei, R.; Li, Q.; Wang, W.J.; Wang, J.C.; Wang, X.L.; Xie, C.Y.; Luo, G.-N. Microstructure and Properties of W-Cu/CuCrZr/316L Joint Bonded by One-Step HIP Technique. *Fusion Eng. Des.* **2018**, *128*, 47–52. [CrossRef]

123. Lee, D.W.; Bae, Y.D.; Kim, S.K.; Hong, B.G.; Jung, H.K.; Park, J.Y.; Jeong, Y.H.; Choi, B.K. High Heat Flux Test with Hip Bonded 50×50 Be/Cu Mock-Ups for the Iter First Wall. *Fusion Sci. Technol.* **2009**, *56*, 48–51. [CrossRef]

124. Ivanov, A.D.; Sato, S.; Le Marois, G. Evaluation of Hot Isostatic Pressing for Joining of Fusion Reactor Structural Components. *J. Nucl. Mater.* **2000**, *283–287*, 35–42. [CrossRef]

125. Orsag, M.; Bogdan, S. Hybrid Control of Quadrotor. In Proceedings of the 2009 17th Mediterranean Conference on Control and Automation, Thessaloniki, Greece, 24–26 June 2009; IEEE: Piscataway, NJ, USA; Volume 1, pp. 1239–1244. [CrossRef]

126. Madhusudhan Reddy, G.; Mohandas, T.; Sambasiva Rao, A.; Satyanarayana, V.V. Influence of welding processes on microstructure and mechanical properties of dissimilar austenitic-ferritic stainless steel welds. *Mater. Manuf. Process.* **2005**, *20*, 147–173. [CrossRef]

127. Senthilkumar, G.; Ramakrishnan, R. Design of Optimal Parameter for Solid-State Welding of EN 10028-P355 GH Steel Using Gray Incidence Reinforced Response Surface Methodology. *Arab. J. Sci. Eng.* **2021**, *46*, 2613–2628. [CrossRef]

128. Carlone, P.; Astarita, A.; Palazzo, G.S.; Paradiso, V.; Squillace, A. Microstructural Aspects in Al–Cu Dissimilar Joining by FSW. *Int. J. Adv. Manuf. Technol.* **2015**, *79*, 1109–1116. [CrossRef]

129. Parikh, V.K.; Badgujar, A.D.; Ghetiya, N.D. Joining of Metal Matrix Composites Using Friction Stir Welding: A Review. *Mater. Manuf. Process.* **2019**, *34*, 123–146. [CrossRef]

130. Marques, E.S.V.; Silva, F.J.G.; Pereira, A.B. Comparison of Finite Element Methods in Fusion Welding Processes—A Review. *Metals* **2020**, *10*, 75. [CrossRef]

131. Annamalai, A.; Babu, T.R.K.; Karthikeyan, S.; Siddharth, N.; Muralidharan, S. *Study of Friction Stir Welding on Aerospace Grade ZE41AMg Alloy and Its Comparison with Laser Beam Welding on ZE41AMg Alloy*; Springer: Singapore, 2021. [CrossRef]

132. DebRoy, T.; Bhadeshia, H.K.D.H. Stirring Solid Metals to Form Sound Welds. In *Innovations in Everyday Engineering Materials*; Springer International Publishing: Cham, Switzerland, 2021. [CrossRef]

133. Aminzadeh, A.; Parvizi, A.; Safdarian, R.; Rahmatabadi, D. Comparison between Laser Beam and Gas Tungsten Arc Tailored Welded Blanks via Deep Drawing. *Proc. Inst. Mech. Eng. Part B J. Eng. Manuf.* **2021**, *235*, 673–688. [CrossRef]

134. Abdou, M.; Sze, D.; Wong, C.; Sawan, M.; Ying, A.; Morley, N.B.; Malang, S.U.S. Plans and Strategy for ITER Blanket Testing. *Fusion Sci. Technol.* **2005**, *47*, 475–487. [CrossRef]

135. Zinkle, S.J.; Möslang, A.; Muroga, T.; Tanigawa, H. Multimodal Options for Materials Research to Advance the Basis for Fusion Energy in the ITER Era. *Nucl. Fusion* **2013**, *53*, 104024. [CrossRef]

136. Nygren, R.E.; Rognlien, T.D.; Rensink, M.E.; Smolentsev, S.S.; Youssef, M.Z.; Sawan, M.E.; Merrill, B.J.; Eberle, C.; Fogarty, P.J.; Nelson, B.E.; et al. A Fusion Reactor Design with a Liquid First Wall and Divertor. *Fusion Eng. Des.* **2004**, *72*, 181–221. [CrossRef]

137. Chai, K.-B.; Kwon, D.-H. Heat and Particle Load Test Facility Using an Applied-Field MPD Thruster for Studying Fusion Divertor Technology. *Plasma Phys. Control. Fusion* **2020**, *62*, 035007. [CrossRef]

138. Mercy Latha, A.; Ghosh, S.K. A Comprehensive Review of Depressed Collectors of Slow-Wave Devices. *J. Electromagn. Waves Appl.* **2021**, *35*, 95–137. [CrossRef]

139. Kato, I. Status of the T2K Experiment. *J. Phys. Conf. Ser.* **2008**, *136*, 022018. [CrossRef]

140. Chu, D.; Jiang, H.; Deng, H.; Yang, J.; Wang, W. Preliminary Experimental Study on Hypervapotron Heat Transfer for High Heat Flux Components. *IEEE Trans. Plasma Sci.* **2018**, *46*, 1372–1376. [CrossRef]

141. Tao, L.; Hu, C.; Xie, Y. Enhanced Heat Transfer Structure Design for Ion Dump of EAST-NBI System Based on Hypervapotron. In *Volume 2: Plant Systems, Structures, Components and Materials*; American Society of Mechanical Engineers: New York, NY, USA, 2017. [CrossRef]

142. Ghule, K.; Yadav, S.S. Investigation of Boiling inside a Hypervapotron with Different Fin Geometries. In *Proceeding of the 24th National and 2nd International ISHMT-ASTFE Heat and Mass Transfer Conference (IHMTC-2017), Hyderabad, India, 27–30 December 2017*; Begellhouse: Danbury, CT, USA, 2018; pp. 467–474. [CrossRef]

143. Rensing, C.; Grass, G. Escherichia Coli Mechanisms of Copper Homeostasis in a Changing Environment. *FEMS Microbiol. Rev.* **2003**, *27*, 197–213. [CrossRef]

144. Cava, R.J. Structural Chemistry and the Local Charge Picture of Copper Oxide Superconductors. *Science* **1990**, *247*, 656–662. [CrossRef]

145. Cava, R.J.; Batlogg, B.; Krajewski, J.J.; Rupp, L.W.; Schneemeyer, L.F.; Siegrist, T.; VanDover, R.B.; Marsh, P.; Peck, W.F.; Gallagher, P.K.; et al. Superconductivity near 70 K in a New Family of Layered Copper Oxides. *Nature* **1988**, *336*, 211–214. [CrossRef]

146. Richardson, C.; Steel, P.J. Benzotriazole as a Structural Component in Chelating and Bridging Heterocyclic Ligands; Ruthenium, Palladium, Copper and Silver Complexes. *Dalt. Trans.* **2003**, *5*, 992–1000. [CrossRef]

147. Ye, X.B.; He, Z.H.; Pan, B.C. The Thermal Conductivity of Defected Copper at Finite Temperatures. *J. Mater. Sci.* **2020**, *55*, 4453–4463. [CrossRef]

148. Muroga, T.; Noto, H.; Hishinuma, Y.; Huang, B. Technical Advancement in Fabricating Dispersion Strengthened Copper Alloys by Mechanical Alloying and Hot Isostatic Pressing for Application to Divertors of Fusion Reactors. *Mater. Sci. Forum* **2018**, *941*, 778–783. [CrossRef]

149. Ye, C. Experimental Investigation of Copper/Stainless Steel Joints Formed by Vacuum Brazing. In Proceedings of the 18th International Conference on Nuclear Engineering: Volume 5, ASMEDC, Xi'an, China, 17–21 May 2010; pp. 47–55. [CrossRef]

150. Swami, H.L.; Danani, C.; Shaw, A.K. Activation Characteristics of Candidate Structural Materials for a Near-Term Indian Fusion Reactor and the Impact of Their Impurities on Design Considerations. *Plasma Sci. Technol.* **2018**, *20*, 065602. [CrossRef]

151. Ali, N.M.; Saeed, A.; El Shazly, R.M.; Al-Fiki, S.A.; Eissa, M.M.; El-kameesy, S.U. Attenuation Effectiveness of Double Phase Stainless Steel Alloys for Fusion Reactor System. *IOP Conf. Ser. Mater. Sci. Eng.* **2020**, *956*, 012008. [CrossRef]

152. Tamura, H.; Yanagi, N.; Goto, T.; Miyazawa, J.; Tanaka, T.; Sagara, A.; Ito, S.; Hashizume, H. Mechanical Design Concept of Superconducting Magnet System for Helical Fusion Reactor. *Fusion Sci. Technol.* **2019**, *75*, 384–390. [CrossRef]

153. Şahin, S.; Şahin, H.M.; Şahiner, H.; Tunç, G. Study on the Fusion Reactor Performance with Different Materials and Nuclear Waste Actinides. *Int. J. Energy Res.* **2020**, *45*, 11759–11774. [CrossRef]

154. Lee, D.W.; Bae, Y.D.; Hong, B.G.; Wang, S.J.; Park, J.Y.; Jeong, Y.H.; Jeong, H.K.; Lee, J.H. Development of Fabrication and Qualification Methods for the First Wall of the International Thermonuclear Experimental Reactor. *J. Korean Phys. Soc.* **2007**, *51*, 1210. [CrossRef]

155. Nishi, H.; Araki, T.; Eto, M. Diffusion Bonding of Alumina Dispersion-Strengthened Copper to 316 Stainless Steel with Interlayer Metals. *Fusion Eng. Des.* **1998**, *39–40*, 505–511. [CrossRef]

156. Sabetghadam, H.; Hanzaki, A.Z.; Araee, A. Diffusion Bonding of 410 Stainless Steel to Copper Using a Nickel Interlayer. *Mater. Charact.* **2010**, *61*, 626–634. [CrossRef]

157. Goods, S.H.; Puskar, J.D. Solid State Bonding of CuCrZr to 316L Stainless Steel for ITER Applications. *Fusion Eng. Des.* **2011**, *86*, 1634–1638. [CrossRef]

158. CUI, Y.; XU, C.; HAN, Q. Effect of Ultrasonic Vibration on Unmixed Zone Formation. *Scr. Mater.* **2006**, *55*, 975–978. [CrossRef]

159. Desai, N.B.; Kedare, S.B.; Bandyopadhyay, S. Optimization of Design Radiation for Concentrating Solar Thermal Power Plants without Storage. *Sol. Energy* **2014**, *107*, 98–112. [CrossRef]

160. Vairis, A.; Frost, M. Design and Commissioning of a Friction Welding Machine. *Mater. Manuf. Process.* **2006**, *21*, 766–773. [CrossRef]
161. Bayindir, R.; Ates, H. Comparison of the Constructed Control Methods for a Friction-Welding Machine. *Mater. Manuf. Process.* **2005**, *20*, 131–146. [CrossRef]
162. Msomi, V.; Moni, V. The Influence of Materials Positioning on Microstructure and Mechanical Properties of Friction Stir Welded AA5083/AA6082 Dissimilar Joint. *Adv. Mater. Process. Technol.* **2021**, 1–15. [CrossRef]
163. Das, D.; Jaypuria, S.; Pratihar, D.K.; Roy, G.G. Weld Optimisation. *Sci. Technol. Weld. Join.* **2021**, *26*, 181–195. [CrossRef]
164. Rehman, A.U.; Babu, N.K.; Talari, M.K.; Usmani, Y.S.; Al-Khalefah, H. Microstructure and Mechanical Properties of Dissimilar Friction Welding Ti-6Al-4V Alloy to Nitinol. *Metals* **2021**, *11*, 109. [CrossRef]
165. Srinivas, K.; Saranarayanan, R.; Lakshminarayanan, A.K.; Srinivasan, N.; Venkatraman, B. Zone Wise Properties of Friction Stir Welded Copper—Stainless Steel Joints Using Digital Image Correlation. *Appl. Mech. Mater.* **2015**, *787*, 485–489. [CrossRef]
166. Murr, L.E. A Review of FSW Research on Dissimilar Metal and Alloy Systems. *J. Mater. Eng. Perform.* **2010**, *19*, 1071–1089. [CrossRef]
167. Wan, L.; Huang, Y. Friction Stir Welding of Dissimilar Aluminum Alloys and Steels: A Review. *Int. J. Adv. Manuf. Technol.* **2018**, *99*, 1781–1811. [CrossRef]
168. Mehta, K.P.; Badheka, V.J. Effects of Tilt Angle on the Properties of Dissimilar Friction Stir Welding Copper to Aluminum. *Mater. Manuf. Process.* **2016**, *31*, 255–263. [CrossRef]
169. Mehta, K.P.; Badheka, V.J. Influence of Tool Design and Process Parameters on Dissimilar Friction Stir Welding of Copper to AA6061-T651 Joints. *Int. J. Adv. Manuf. Technol.* **2015**, *80*, 2073–2082. [CrossRef]
170. Windows, M.; Os, M.; When, C.P.; Wei, Y.; Yildirim, P.; den Bulte, C.; Dellarocas, C.; Weekly, T.; Weekly, I.C.T.I.; Henley, W.E.; et al. *Advances in Friction Stir Welding and Proccessing*; Woodhead Publishing: Sawston, UK, 2014; Volume XXXIII. [CrossRef]
171. Mehta, K.P.; Badheka, V.J. A Review on Dissimilar Friction Stir Welding of Copper to Aluminum: Process, Properties, and Variants. *Mater. Manuf. Process.* **2016**, *31*, 233–254. [CrossRef]
172. Ahmad Shah, L.H.; Midawi, A.; Walbridge, S.; Gerlich, A. Influence of Tool Offsetting and Base Metal Positioning on the Material Flow of AA5052-AA6061 Dissimilar Friction Stir Welding. *J. Mech. Eng. Sci.* **2020**, *14*, 6393–6402. [CrossRef]
173. Mallieswaran, K.; Padmanabhan, R. Effect of Sheet Thickness on the FSW Parameters for Dissimilar Aluminium Grades Tailor Welded Blanks. *Adv. Mater. Process. Technol.* **2020**, *7*, 1–16. [CrossRef]
174. Kasman, S. The Effects of Pin Offset for FSW of Dissimilar Materials: A Study for AA 7075—AA 6013. *Matéria* **2020**, *25*, 1–14. [CrossRef]
175. Ghiasvand, A.; Kazemi, M.; Mahdipour Jalilian, M.; Ahmadi Rashid, H. Effects of Tool Offset, Pin Offset, and Alloys Position on Maximum Temperature in Dissimilar FSW of AA6061 and AA5086. *Int. J. Mech. Mater. Eng.* **2020**, *15*, 6. [CrossRef]
176. Thomas, W.M.; Threadgill, P.L.; Nicholas, E.D. Feasibility of Friction Stir Welding Steel. *Sci. Technol. Weld. Join.* **1999**, *4*, 365–372. [CrossRef]
177. Zhang, Y.N.; Cao, X.; Larose, S.; Wanjara, P. Review of Tools for Friction Stir Welding and Processing. *Can. Metall. Q.* **2012**, *51*, 250–261. [CrossRef]
178. Prater, T. Solid-State Joining of Metal Matrix Composites: A Survey of Challenges and Potential Solutions. *Mater. Manuf. Process.* **2011**, *26*, 636–648. [CrossRef]
179. Chandrashekar, A.; Kumar, B.S.A.; Reddappa, H.N. Friction Stir Welding: Tool Material and Geometry. *AKGEC Int. J. Technol.* **2015**, *6*, 16–20.
180. Shindo, D.J.; Rivera, A.R.; Murr, L.E. Shape Optimization for Tool Wear in the Friction-Stir Welding of Cast Al359-20% SiC MMC. *J. Mater. Sci.* **2002**, *37*, 4999–5005. [CrossRef]
181. Eff, M. *The Effects of Tool Texture on Tool Wear in Friction Stir Welding of X-70 Steel*; The Ohio State University: Columbus, OH, USA, 2012.
182. Tiwari, A.; Pankaj, P.; Suman, S.; Singh, P.; Biswas, P.; Pal, S.; Rao, A.G. Effect of Plasma Preheating on Weld Quality and Tool Life during Friction Stir Welding of DH36 Steel. *Proc. Inst. Mech. Eng. Part B J. Eng. Manuf.* **2021**, *235*, 1458–1472. [CrossRef]
183. Lauterbach, D.; Keil, D.; Harms, A.; Leupold, C.; Dilger, K. Tool Wear Behaviour and the Influence of Wear-Resistant Coatings during Refill Friction Stir Spot Welding of Aluminium Alloys. *Weld. World* **2021**, *65*, 243–250. [CrossRef]
184. Vicharapu, B.; Lemos, G.V.B.; Bergmann, L.; dos Santos, J.F.; De, A.; Clarke, T. Probing Underlying Mechanisms for PCBN Tool Decay during Friction Stir Welding of Nickel-Based Alloys. *Tecnol. em Metal. Mater. Min.* **2021**, *18*, e2455. [CrossRef]
185. Stewart, H.A. Cryogenic Treatment of Tungsten Carbide Reduces Tool Wear When Machining Medium Density Fiberboard. *For. Prod. J.* **2004**, *54*, 53–56.
186. Gill, S.S.; Singh, J.; Singh, H.; Singh, R. Metallurgical and Mechanical Characteristics of Cryogenically Treated Tungsten Carbide (WC–Co). *Int. J. Adv. Manuf. Technol.* **2012**, *58*, 119–131. [CrossRef]
187. Gill, S.S.; Singh, J.; Singh, R.; Singh, H. Metallurgical Principles of Cryogenically Treated Tool Steels—A Review on the Current State of Science. *Int. J. Adv. Manuf. Technol.* **2011**, *54*, 59–82. [CrossRef]
188. Akıncıoğlu, G. Investigation of the Effect of Cryogenic Treatment Cubic Boron Nitride Turning Insert Tools. *J. Mater. Eng. Perform.* **2021**, *30*, 1280–1288. [CrossRef]
189. Yooliengpun, C.; Bandasak, N.; Tuchinda, K.; Diewwanit, O. Effect of Cryogenic Treatment of Cemented Tungsten Carbide Tools for Die Application. *IOP Conf. Ser. Mater. Sci. Eng.* **2021**, *1048*, 012002. [CrossRef]

190. Parida, B.; Vishwakarma, S.D.; Pal, S. Design and Development of Fixture and Force Measuring System for Friction Stir Welding Process Using Strain Gauges. *J. Mech. Sci. Technol.* **2015**, *29*, 739–749. [CrossRef]

191. Yaduwanshi, D.K.; Bag, S.; Pal, S. Hybrid Friction Stir Welding of Similar and Dissimilar Materials. In Proceedings of the 5th international and 26th all India Manufacturing Technology, Delhi, India, 12–14 December 2014; pp. 323–347.

192. Yaduwanshi, D.K.; Bag, S.; Pal, S. On the Effect of Tool Offset in Hybrid-FSW of Copper-Aluminium Alloy. *Mater. Manuf. Process.* **2018**, *33*, 277–287. [CrossRef]

193. Sinclair, P.C.; Longhurst, W.R.; Cox, C.D.; Lammlein, D.H.; Strauss, A.M.; Cook, G.E. Heated Friction Stir Welding: An Experimental and Theoretical Investigation into How Preheating Influences Process Forces. *Mater. Manuf. Process.* **2010**, *25*, 1283–1291. [CrossRef]

194. Kim, K.-H.; Bang, H.-S.; Ro, C.-S.; Bang, H.-S. Influence of Preheating Source on Mechanical Properties and Welding Residual Stress Characteristics in Ultra Thin Ferritic Stainless Steel Hybrid Friction Stir Welded Joints. *Int. J. Precis. Eng. Manuf. Technol.* **2017**, *4*, 393–400. [CrossRef]

195. Joo, S. Joining of Dissimilar AZ31B Magnesium Alloy and SS400 Mild Steel by Hybrid Gas Tungsten Arc Friction Stir Welding. *Met. Mater. Int.* **2013**, *19*, 1251–1257. [CrossRef]

196. Liu, H.J.; Zhang, H.J. Study of Hybrid Welding Repair Process of Friction Stir Welding Grove Defect. *Sci. Technol. Weld. Join.* **2012**, *17*, 169–173. [CrossRef]

197. Li, X.; Chen, S.; Yuan, T.; Jiang, X.; Han, Y. Improving the Properties of Friction Stir Welded 2219-T87 Aluminum Alloy with GTA Offset Preheating. *J. Manuf. Process.* **2020**, *51*, 10–18. [CrossRef]

198. Satpathy, M.P.; Kumar, A.; Sahoo, S.K. Effect of Brass Interlayer Sheet on Microstructure and Joint Performance of Ultrasonic Spot-Welded Copper-Steel Joints. *J. Mater. Eng. Perform.* **2017**, *26*, 3254–3262. [CrossRef]

199. Kore, S.D.; Date, P.P.; Kulkarni, S.V.; Kumar, S.; Rani, D.; Kulkarni, M.R.; Desai, S.V.; Rajawat, R.K.; Nagesh, K.V.; Chakravarty, D.P. Application of Electromagnetic Impact Technique for Welding Copper-to-Stainless Steel Sheets. *Int. J. Adv. Manuf. Technol.* **2011**, *54*, 949–955. [CrossRef]